Phase Retrieval for $L^2([-\pi, \pi])$ via the Provably Accurate and Noise Robust Numerical Inversion of Spectrogram Measurements

Mark Iwen[1], Michael Perlmutter[2*], Nada Sissouno[3] and Aditya Viswanathan[4]

[1]Department of Mathematics, and the Department of Computational Mathematics, Science and Engineering (CMSE), Michigan State University, 619 Red Cedar Road, East Lansing, 48824, MI, USA.

[2*]Department of Mathematics, University of California, Los Angeles, 520 Portola Plaza, Los Angeles, 90095, CA, USA.

[3]Faculty of Mathematics, TUM & DIG Strategy and Digitalization, Helmholtz Zentrum München, TUM: Technical University of Munich, 3 Boltzmannstrasse, Garching b. München, 85748, Bavaria, Germany.

[4]Department of Mathematics & Statistics, University of Michigan – Dearborn, 4901 Evergreen Road, Dearborn, 48128, MI, USA.

*Corresponding author(s). E-mail(s): perlmutter@math.ucla.edu; Contributing authors: markiwen@math.msu.edu; sissouno@ma.tum.de; adityavv@umich.edu;

Abstract

In this paper, we focus on the approximation of smooth functions $\boldsymbol{f} : [-\boldsymbol{\pi}, \boldsymbol{\pi}] \to \mathbb{C}$, up to an unresolvable global phase ambiguity, from a finite set of Short Time Fourier Transform (STFT) magnitude (i.e., spectrogram) measurements. Two algorithms are developed for approximately inverting such measurements, each with theoretical error guarantees establishing their correctness. A

detailed numerical study also demonstrates that both algorithms work well in practice and have good numerical convergence behavior.

Keywords: Phase Retrieval, Ptychography, STFT Magnitude Measurements, Spectrogram Measurements

1 Introduction

We consider the approximate recovery of a smooth function $f : \mathbb{R} \to \mathbb{C}$, supported inside of a compact interval $I \subset \mathbb{R}$, from a finite set of noisy spectrogram measurements of the form

$$Y_{\omega,\ell} := \left| \int_{-\infty}^{\infty} f(x)\tilde{m}\left(x - \frac{2\pi}{L}\ell\right) \mathrm{e}^{-\mathrm{i}x\omega} dx \right|^2 + \eta_{\omega,\ell}. \tag{1}$$

Here $\tilde{m} : \mathbb{R} \to \mathbb{C}$ is a known mask, or window, and the $\eta_{\omega,\ell}$ are arbitrary additive measurement errors. Without loss of generality, we will assume that $I \subset (-\pi, \pi)$ and seek to characterize how well the function f, with its domain restricted to $[-\pi, \pi]$, can be approximated using dL measurements of this form for d frequencies ω at each of L shifts ℓ. Toward that end, we present two algorithms which can provably approximate any such function f (belonging to a general regularity class defined below in Definition 1.4) up to a global phase multiple using spectrogram measurements of this type resulting from two different types of masks $\tilde{m}$. As we shall see, both algorithms ultimately work by approximating finitely many Fourier series coefficients of $f|_{[-\pi,\pi]}$.[1]

Inverse problems of this type appear in many applications including optics [1], astronomy [2], and speech signal processing [3, 4] to name just a few. In this paper we are primarily motivated by phaseless imaging applications such as ptychography [5], in which Fourier magnitude data is collected from overlapping shifts of a mask/probe (e.g., a pinhole) across a specimen and then used to recover the specimen's image. Indeed, these types of phaseless imaging applications directly motivate the types of masks $\tilde{m} : \mathbb{R} \to \mathbb{C}$ considered below. In particular, we consider two types of masks $\tilde{m}$ including both (i) relatively low-degree trigonometric polynomial masks representing masking the sample f with shifts of a periodic structure/grating, and (ii) compactly supported masks representing the translation of, e.g., an aperture/pinhole across the sample during imaging. Note that first type of periodic masks are reminicent of some of the Coded Diffraction Pattern type measurements for phase retrieval

[1] Given $f : \mathbb{R} \to \mathbb{C}$, let $f|_{[-\pi,\pi]}$ be f with its domain restricted to $[-\pi, \pi]$. Note that the Fourier transform of a function $f \in L^2(\mathbb{R})$ with support in $(-\pi, \pi)$ yields, when evaluated on the integers, the Fourier series coefficients of $f|_{[-\pi,\pi]}$ up to a 2π factor. Using this relationship, we aim herein to approximate such functions on $[-\pi, \pi]$ using trigonometric polynomials. In a minor abuse of notation motivated by this strategy, we will use $\hat{f}$ to refer to two related objects in this section: $\hat{f}$ will refer to both the suitably renormalized Fourier transform of f as a function on $\mathbb{R}$, and, when restricted to $\mathbb{Z}$, to the Fourier series coefficients of $f|_{[-\pi,\pi]}$ defined as per (9).

analyzed by Candès et al. in the discrete (i.e., finite-dimensional f and $\tilde{m}$) setting [6, 7]. (See Section 1 of [8] for a related discussion.) The second type of compactly supported masks, on the other hand, correspond more closely to standard ptychographic setups in which Fourier magnitude data is collected from small overlapping portions of a large sample f in order to eventually recover its global image.

Although a number of algorithms exhibiting great empirical success were designed decades ago for phaseless imaging, e.g., [9], [10], [3], the mathematical community has only recently begun to undertake the challenge of designing measurement setups and corresponding recovery algorithms with provable accuracy and reconstruction guarantees. The vast majority of those theoretical works, which propose and analyze numerical algorithms, have only addressed discrete (i.e., finite-dimensional) phase retrieval problems, (see e.g., [4], [11], [6], [7], [12], [13]) where the signal of interest and measurement masks are both discrete vectors and where the relevant measurement vectors are generally random and globally supported. (We do however note that there has been a large body of work (such as [14–16]) on the non-algorithmic aspects of phase retrieval in the continuous setting. For an overview of this work, please see [17] and the references within.)

In this paper, we develop a provably accurate numerical method[2] for approximating smooth functions $f : \mathbb{R} \to \mathbb{C}$ from a finite set of Short-Time Fourier Transform (STFT) magnitude measurements. Though there has been general work concerning the uniqueness and stability of reconstruction from STFT magnitude measurements in this setting (see, e.g., recent work by Alaifari, Cheng, Daubechies, and their collaborators [18], [19]), to the best of our knowledge, no prior work exists concerning the development or analysis of provably accurate numerical methods for actually carrying out such reconstructions from a finite set of such measurements. Perhaps the closest prior work is that of Thakur [20], who gives an algorithm for the reconstruction of real-valued bandlimited functions up to a global sign from the absolute values of their point samples, and that of Gröchenig [21], who considers/surveys similar results in shift-invariant spaces. Other related work includes that of Alaifari et al. [22], which proves (among other things) that one can not hope to stably recover a periodic function up to a single global phase using a trigonometric polynomial mask of degree $\rho/2$, as done below, unless its Fourier series coefficients do not vanish on any ρ consecutive integer frequencies in between two other frequencies with nonzero Fourier series coefficients. This helps to motivate the function classes we consider recovering here. (In particular, if a function f satisfies Definition 1.4 below, then any strings of zero Fourier series coefficients in $\{\hat{f}(n)\}_{n\in\mathbb{Z}}$ longer than a certain finite length must be part of an infinite string of zero Fourier coefficients associated with all frequencies beyond a finite cutoff.) We also refer the reader to [23] and [19] for similar considerations in the discrete setting.

[2]Numerical implementations of the methods proposed here are available at https://bitbucket.org/charms/blockpr.

1.1 Problem Setup and Main Results

Let $\tilde{m}, f : \mathbb{R} \to \mathbb{C}$ be C^k-functions for some $k \geq 2$, d be an odd number, and let K and L both divide d. Furthermore, let $\mathcal{D} = \{-\frac{d-1}{2}, \ldots, 0, \ldots, \frac{d-1}{2}\}$, and choose $\Omega, \mathcal{L}' \subseteq \mathcal{D}$ with $|\Omega| = K$ and $|\mathcal{L}'| = L$. Finally, let $\mathbf{Y}_{K,L}$ be the $K \times L$ measurement matrix defined by

$$(\mathbf{Y}_{K,L})_{\omega,\ell} := \left| \int_{\mathbb{R}} f(x)\tilde{m}\left(x - \frac{2\pi}{d}\ell\right) \mathrm{e}^{-\mathrm{i}x\omega} dx \right|^2 + \eta_{\omega,\ell}, \tag{2}$$

for all $(\omega, \ell) \in \Omega \times \mathcal{L}'$, where $\boldsymbol{\eta}_{\mathbf{K},\mathbf{L}} = (\eta_{\omega,\ell})_{(\omega,\ell)\in\Omega\times\mathcal{L}'}$ is an arbitrary additive noise matrix on the acquired samples. The goal of this paper is to begin to address the following question.

Question 1.1 *Under what conditions on f, $\tilde{m}$, Ω, and $\mathcal{L}'$ can we produce an efficient and noise robust algorithm which provably recovers f from the $K \times L$ matrix $\mathbf{Y}_{K,L}$ of acquired measurements?*

In order to partially answer this question, we will assume that f satisfies a regularity assumption defined below in Definition 1.4 and also that one of the following two (mutually exclusive) assumptions holds:

Assumption 1.2 *f is compactly supported with $supp(f) \subset (-\pi, \pi)$ and $\tilde{m}$ is a trigonometric polynomial given by*

$$\tilde{m}(x) = \sum_{p=-\rho/2}^{\rho/2} \widehat{m}(p)\mathrm{e}^{\mathrm{i}px}$$

for some even number $\rho < d/2$ and some $\widehat{m}(-\rho/2), \ldots, \widehat{m}(0), \ldots, \widehat{m}(\rho/2) \in \mathbb{C}$.

Assumption 1.3 *Both f and $\tilde{m}$ are compactly supported with $supp(f) \subset (-a, a)$ and $supp(\tilde{m}) \subset (-b, b)$ for some a and b such that $a + b \leq \pi$.*

We will introduce a four-step method which relies on recovering the Fourier coefficients of f. Our first step is to carefully discretize the problem. Rather than simply constructing a vector from pointwise samples, our discretization step is based up approximating the mask $\tilde{m}$ restricted to $[-\pi, \pi]$ by a function with finitely many nonzero Fourier series coefficients. Therefore, we effectively regard the mask as being compactly supported in the frequency domain. As mentioned above, several previous works, including [19], [22], and [23], have noted that this implies that the recovery of f is impossible if f has many consecutive Fourier coefficients which are equal to zero followed by nonzero Fourier coefficients at higher frequencies. Moreover, if there are many consecutive small Fourier coefficients followed by larger coefficients at higher frequencies, the problem is inherently unstable. Therefore, we will remove such pathological

functions from consideration by assuming that our function f is a member of the following function class for a suitable choice of β. This choice of β will depend on whether f and $\tilde{m}$ satisfy Assumption 1.2 or Assumption 1.3, respectively.

Definition 1.4 *Let $f \in L^2(\mathbb{R})$ with $supp(f) \subset (-\pi, \pi)$. Let β be a positive integer and let $D_n := \max_{m \in \mathbb{Z} \text{ s.t. } |m-n|<\beta/2} |\widehat{f}(m)|$ for all $n \in \mathbb{Z}$. We say that f has β* Fourier decay *if $D_n \geq D_{n'}$ whenever $|n| \leq |n'|$. Additionally, for $k \geq 1$, we shall let $\mathcal{C}_\beta^k$ denote the set of all compactly supported functions $f : \mathbb{R} \to \mathbb{C}$ with $supp(f) \subset (-\pi, \pi)$ that are C^k-smooth and have β Fourier Decay.*

In particular, we note that if $|\widehat{f}(n)|$ is decreasing in $|n|$, then the conditions of Definition 1.4 are automatically satisfied for any β. We also note a useful property of this function class, which follows immediately from the definition, in the following remark.

Remark 1.5 *Suppose f has β Fourier decay for some integer β, and let $a, n \in \mathbb{Z}$ with $|a| < |n|$. Then, if β is odd, the string of β consecutive integers centered around a contains an integer m such that $|\widehat{f}(m)| \geq |\widehat{f}(n)|$. Similarly, if β is even, then the string of $\beta - 1$ consecutive integers centered around a contains an integer m such that $|\widehat{f}(m)| \geq |\widehat{f}(n)|$.*

We will show that functions satisfying Definition 1.4 can be reconstructed from a matrix $\mathbf{Y}$, whose entries $Y_{\omega,\ell}$ are defined as in (1), using the following four-step approach:

1. Approximate the matrix of continuous measurements $\mathbf{Y}$, defined in terms of functions f and $\tilde{m}$, by a matrix of discrete measurements $\mathbf{T}$ defined in terms of vectors corresponding to the first s Fourier coefficients of f and the first r coefficients of $\tilde{m}$.
2. Apply a discrete Wigner distribution deconvolution method [8] to recover a portion of the Fourier autocorrelation matrix $\widehat{\mathbf{x}}\widehat{\mathbf{x}}^*$, where $\widehat{\mathbf{x}}$ is a vector whose entries approximate the Fourier coefficients of f.
3. Recover $\widehat{\mathbf{x}}$ via a greedy angular synchronization scheme along the lines of the one used in [24].
4. Estimate f by a trigonometric polynomial with coefficients given by $\widehat{\mathbf{x}}$.

The details of step 2 are quite different depending on whether f and $\tilde{m}$ satisfy Assumption 1.2 or Assumption 1.3. However, we emphasize that the other three steps of the process are identical in either case. The result of this approach is two algorithms which allow for the reconstruction of f under either Assumption 1.2 or 1.3, as well as accompanying theoretical results providing convergence guarantees. The following theorems are simplified variants of our main results Corollaries 4.2 and 4.3 presented in Section 4. Details on how to deduce these results from Corollaries 4.2 and 4.3 are provided in Section 4.

Theorem 1.6 (Trigonometric Polynomial Masks) *Let k and ρ be integers with $k \geq 5$ and ρ even. Let $K = d \geq 2\rho + 6$, and let L divide d with $2 + \rho \leq L \leq 2\rho$. Let $\mathbf{Y}_{d,L}$ be the $d \times L$ measurement matrix defined in (2) with Ω and $\mathcal{L}'$ chosen to be as in (6). Then there exist degree $\rho/2$ trigonometric polynomial masks $\tilde{m}$ and an efficient numerical algorithm (described in detail by Algorithm 1) such that for all $f \in \mathcal{C}^k_{\rho/2}$ this algorithm outputs a trigonometric polynomial $f_e(x)$ guaranteed to satisfy*

$$\min_{\theta \in [0,2\pi]} \left\| e^{\mathbb{i}\theta} f - f_e \right\|^2_{L^2([-\pi,\pi])} \leq C_{f,m} \left(\left(\frac{1}{d} \right)^{k-9/2} + \frac{d^3}{L^{1/2}} \|\boldsymbol{\eta}_{\mathbf{d},\mathbf{L}}\|_F \right),$$

where $\boldsymbol{\eta}_{\mathbf{d},\mathbf{L}}$ is the $d \times L$ additive noise matrix defined in (2), and $C_{f,m}$ is a constant only depending on $f, \widetilde{m}$, and k.

Theorem 1.6 guarantees the existence of periodic masks which allow the exact recovery of all sufficiently smooth f as above as $d \to \infty$ in the noiseless case (i.e., when $\boldsymbol{\eta}_{\mathbf{d},\mathbf{L}} = \mathbf{0}$). In particular, it is shown that a single mask $\tilde{m}$ will work with all sufficiently large choices of d as long as d has a divisor in $[\rho + 2, 2\rho]$. Furthermore, Theorem 1.6 demonstrates that Algorithm 1 is robust to small amounts of arbitrary additive noise on its measurements for any fixed d. We note here that the d^3 term in front of the noise term $\|\boldsymbol{\eta}_{\mathbf{d},\mathbf{L}}\|_F$ is almost certainly highly pessimistic, and the numerical results in Section 5 indicate that the method performs well with noisy measurements in practice. We expect that this d^3 dependence in our theory can be reduced, especially for more restricted classes of functions f that are compatible with less naive angular synchronization approaches than the one utilized here. (See, for example, recent work on angular synchronization approaches for phase retrieval by Filbir et al. [25].) Finally we note that Theorem 1.6 may also be applied to masks $\widetilde{m}$ obtained by multiplying a trigonometric polynomial by $\mathbb{1}_{[-3\pi,3\pi]}$, the characteristic function of the set $[-3\pi, 3\pi]$. Indeed, given that f is itself compactly supported, any support restrictions on the mask $\widetilde{m}$ which leave the support of f entirely contained within the support of all the utilized shifts of $\widetilde{m}$ will not change our measurements (2). This suggests that periodic masks whose physical extent includes the sample being imaged may be useful for phaseless imaging in practice.

Focusing on the total number of STFT magnitude measurements (2) used by Algorithm 1, we can see that Theorem 1.6 guarantees that $KL \leq 2d\rho$ will suffice for accurate reconstruction when the mask $\tilde{m}$ is a trigonometric polynomial. In particular, this is linear in d for a fixed ρ. As we shall see below, the situation appears more complicated when $\tilde{m}$ is compactly supported. In particular, Theorem 1.8 stated below requires $KL = d^2/3$ STFT magnitude measurements in that setting (and more generally, the argument we give here always requires $KL \geq Cbd^2$, where C is an absolute constant, and b is the support size of the mask as per Assumption 1.3). Before stating Theorem 1.8, we will introduce the following function class.

Definition 1.7 *For $a \in (0, \pi - 3/4)$ and $k \geq 4$, let $\tilde{\mathcal{C}}^k_{a,\beta}$ be the set of all compactly supported functions $f : \mathbb{R} \to \mathbb{C}$ with $supp(f) \subseteq (-a, a)$ that are C^k-smooth and have β Fourier decay.*

Theorem 1.8 (Compactly Supported Masks) *Let $a \in (0, \pi - 3/4)$, $b = 3/4$, $K = d/3$, and fix $d = L$ to be a multiple of three large enough that all of the following hold: $\beta < \lceil db/2\pi \rceil - 1/2$, $s = r = \lceil db/2\pi \rceil < d/8 - 1$, and $5d/21 < \delta = \lfloor db/\pi \rfloor < d/4$. Let $\mathbf{Y}_{K,d}$ be the $K \times d$ measurement matrix defined in (2) with Ω and $\mathcal{L}'$ chosen to be as in (6). Then, there exists an efficient numerical algorithm (described in detail in Algorithm 2), such that for any compactly supported mask $\tilde{m}$ with $supp(\tilde{m}) \subseteq (-b, b)$ and $\mu_2 > 0$ (see (36) and (13) for the definition of μ_2) the trigonometric polynomial $f_e(x)$ output this algorithm is guaranteed to satisfy*

$$\min_{\theta \in [0,2\pi]} \left\| \mathfrak{e}^{\mathfrak{i}\theta} f - f_e \right\|^2_{L^2([-\pi,\pi])} \leq C_{f,m} \left(\frac{1}{\mu_2 \sigma_{\min}(\mathbf{W}) d^k} + \frac{\|\boldsymbol{\eta}_{\mathbf{K},\mathbf{d}}\|_F}{\mu_2 \sigma_{\min}(\mathbf{W})} + \left(\frac{1}{d}\right)^{2k-2} \right)$$

for all $f \in \tilde{\mathcal{C}}^k_{a,\beta}$, where $C_{f,m}$ is a constant only depending on $f, \widetilde{m}$, and k. Here $\sigma_{\min}(\mathbf{W})$ denotes the smallest singular value of the $(2(d/3 - \lfloor 3d/4\pi \rfloor) - 1) \times \lceil db/2\pi \rceil$ partial Fourier matrix $\mathbf{W}$ defined in Section 3.2 and $\boldsymbol{\eta}_{\mathbf{K},\mathbf{d}}$ is the $K \times d$ additive noise matrix defined in (2).

Theorem 1.8 demonstrates that sufficiently smooth functions f can be approximated well for measurement setups and masks having μ_2 and $\sigma_{\min}(\mathbf{W})$ not too small. Furthermore, Proposition 3.4 demonstrates that masks exist for which μ_2 scales polynomially in d (independently of f and k). It remains an open problem, however, to find a single compactly supported mask $\tilde{m}$ which will provably allow recovery for all choices of d, as well as optimal constructions of such masks more generally. Nonetheless, our numerical results in Section 5 demonstrate that Algorithm 2 does indeed work well in practice for a fixed compactly supported mask and that the mask we evaluate has reasonable values of μ_2 for the range of choices of d evaluated there.

1.2 Notation

In this section, we introduce the most essential notation used throughout the paper. We will also provide a table detailing the notation introduced in each chapter at the end of this chapter.

We will denote matrices and vectors by bold letters. We will let $\mathbf{M}_j$ denote the j-th column of a matrix $\mathbf{M}$ and, if $\mathbf{x}$ and $\mathbf{y}$ are vectors, we will let

$$\mathbf{x} \circ \mathbf{y} \quad \text{and} \quad \frac{\mathbf{x}}{\mathbf{y}}$$

denote their componentwise (Hadamard) product and their componentwise quotient. For any odd number n, we will let

$$[n]_c \coloneqq \left[\frac{1-n}{2}, \frac{n-1}{2} \right] \cap \mathbb{Z}$$

be the set of n consecutive integers centered at the origin. In a slight abuse of notation, if n is even, we will define $[n]_c := [n+1]_c$, so that in either case $[n]_c$ is the smallest set of at least n consecutive integers centered about the origin. We will let d be an odd number, let K and L divide d, and let

$$\mathcal{D} := [d]_c, \quad \mathcal{K} := [K]_c, \quad \text{and} \quad \mathcal{L} := [L]_c.$$

For $\ell \in \mathbb{Z}$, we let $S_\ell : \mathbb{C}^d \to \mathbb{C}^d$ be the circular shift operator defined for $\mathbf{x} = (x_p)_{p\in\mathcal{D}}$ by

$$(S_\ell \mathbf{x})_p = \mathbf{x}_{p+\ell}, \tag{3}$$

where the addition $p+\ell$ is interpreted to mean the unique element of $\mathcal{D}$ which is equivalent to $p+\ell$ modulo d.

If K and L are integers which divide d, and $\mathbf{M} = (M_{k,\ell})_{k,\ell\in\mathcal{D}}$ is a $d \times d$ matrix, we will let $\mathbf{M_{K,L}}$ be the $K \times L$ matrix defined by effectively subsampling $\mathbf{M}$ at equally spaced entries. That is, for $k \in \mathcal{K}$ and $\ell \in \mathcal{L}$, we let

$$(\mathbf{M_{K,L}})_{k,\ell} = M_{k\frac{d}{K},\ell\frac{d}{L}}. \tag{4}$$

For the sake of notational convenience and ease of analysis, we will often consider our $K \times L$ measurement matrix $\mathbf{Y}_{K,L}$ in (2) utilized herein to be defined in terms of a subsampling operation applied to a larger $d \times d$ matrix $\mathbf{Y}$ of potential samples in exactly this way. That is, let $\mathbf{Y}$ have entires given by

$$(\mathbf{Y})_{\omega,\ell} := \left| \int_{\mathbb{R}} f(x)\tilde{m}\left(x - \frac{2\pi}{d}\ell\right) \mathrm{e}^{-\mathrm{i}x\omega} dx \right|^2 + \eta_{\omega,\ell}, \tag{5}$$

for all $\omega, \ell \in \mathcal{D}$. Then, we will consider $\mathbf{Y}_{K,L}$ to be defined via (4) as a subsampled version of a larger matrix of potential samples $\mathbf{Y}$. Note that is equivalent to the measurements defined in (2) with Ω and $\mathcal{L}'$ chosen to be

$$\Omega := \{\omega d/K\}_{\omega\in\mathcal{K}} \text{ and } \mathcal{L}' := \{\ell d/L\}_{\ell\in\mathcal{L}}. \tag{6}$$

Remark 1.9 *Note that defining $\mathbf{Y}_{K,L}$ via (2) with Ω and $\mathcal{L}'$ as per (6) is only equivalent to subsampling a larger potential sample matrix $\mathbf{Y}$ above via (4) if one ignores the noise $\eta_{\omega,\ell}$ on the unsampled entires of $\mathbf{Y}$. Indeed, with slight abuse of notation, and for consistency, we will use this subsampling notation (4) even when referring to a $K \times L$ noise matrix. However, there is no subsampling process for noise assumed/used herein, and the notation refers exclusively to the dimensions of the noise matrix when used (with the entries of the noise matrix our algorithms actually utilize defined as per (2) with Ω and $\mathcal{L}'$ chosen as in (6)).*

We let $\mathbf{F_d}$ be the $d \times d$ Fourier matrix with entries given by

$$(\mathbf{F_d})_{j,k} = \frac{1}{d}\mathrm{e}^{\frac{-2\pi\mathrm{i}jk}{d}}$$

for $j, k \in \mathcal{D}$, and similarly let $\mathbf{F_L}$ and $\mathbf{F_K}$ be the $L \times L$ and $K \times K$ Fourier matrices with indices in $\mathcal{L}$ and $\mathcal{K}$, respectively. Finally, we will often use generic constants whose values change from line to line, but whose dependencies on other quantities are explicitly tracked and noted. These constants will be denoted by capital C and have subscripts that indicate the mathematical objects on which they depend.

2 Discretization

Let $\tilde{m}, f : \mathbb{R} \to \mathbb{C}$ be C^k-functions for some $k \geq 2$ such that $\text{supp}(f) \subseteq [-\pi, \pi]$, and assume that either Assumption 1.2 or Assumption 1.3 holds. We will define m to be a periodic function which coincides with $\tilde{m}$ on $[-\pi, \pi]$. Specifically, we let

$$m(x) := \begin{cases} \tilde{m}(x) & \text{if Assumption 1.2 holds,} \\ \sum_{n \in \mathbb{Z}} \tilde{m}(x + 2\pi n) & \text{if Assumption 1.3 holds.} \end{cases}$$

As in Section 1, let $\mathcal{D}$ be the set of d consecutive integers centered at the origin, and define $\mathbf{Z} = (Z_{\omega,\ell})_{\omega,\ell \in \mathcal{D}}$ to be the $d \times d$ matrix with entries given by

$$Z_{\omega,\ell} := \left| \int_{\mathbb{R}} f(x) \tilde{m}\left(x - \frac{2\pi}{d}\ell\right) \mathrm{e}^{-\mathrm{i}x\omega} dx \right|^2.$$

Our goal is to recover f from the matrix $\mathbf{Y} = (Y_{\omega,\ell})_{\omega,\ell \in \mathcal{D}}$ of noisy measurements given by

$$Y_{\omega,\ell} := Z_{\omega,\ell} + \eta_{\omega,\ell},$$

where $\boldsymbol{\eta} = (\eta_{\omega,\ell})_{\omega,\ell \in \mathcal{D}}$ is an arbitrary additive noise matrix. Since the support of f is contained in $[-\pi, \pi]$, we note that

$$Z_{\omega,\ell} = \left| \int_{-\pi}^{\pi} f(x) \tilde{m}\left(x - \frac{2\pi}{d}\ell\right) \mathrm{e}^{-\mathrm{i}x\omega} dx \right|^2. \tag{7}$$

Furthermore, under either Assumption 1.2 or Assumption 1.3, we note that we may replace $\tilde{m}$ with m in (7), i.e.,

$$Z_{\omega,\ell} = \left| \int_{-\pi}^{\pi} f(x) m\left(x - \frac{2\pi}{d}\ell\right) \mathrm{e}^{-\mathrm{i}x\omega} dx \right|^2. \tag{8}$$

Under Assumption 1.2, this is immediate since $\tilde{m}(x) = m(x)$ by definition. Under Assumption 1.3, we note that

$$\text{supp}(\tilde{m} - m) \subseteq (-\infty, b - 2\pi] \cup [2\pi - b, \infty)$$

and that $\left|\frac{2\pi\ell}{d}\right| < \pi$ for all $\ell \in \mathcal{D}$. Therefore, we have that

$$\tilde{m}\left(x - \frac{2\pi}{d}\ell\right) - m\left(x - \frac{2\pi}{d}\ell\right) = 0 \quad \text{for all } |x| < \pi - b.$$

Notation	Notes
Basic notation	
$\mathbf{M}_j$	j-th column of a matrix $\mathbf{M}$
$[n]_c$	set of n consecutive integers centered at the origin
$\mathcal{D} = [d]_c$	for odd d
$\mathcal{K} = [K]_c$	for odd K dividing d
$\mathcal{L} = [L]_c$	for odd L dividing d
$\mathbf{M}_{\mathbf{K},\mathbf{L}}$	$K \times L$ sub-matrix of $\mathbf{M} = (M_{k,\ell})_{k,\ell \in \mathcal{D}}$; see (4)
S_ℓ	circular shift operator; see (3)
$\mathbf{F_d}$	$d \times d$ Fourier matrix
$\widehat{\mathbf{x}} \coloneqq \mathbf{F_d x}$	discrete Fourier transform of a vector $\mathbf{x}$
$\mathbf{Y}$	finite set of noisy spectrogram measurements; see (5)
$\mathbf{Y}_{K,L}$	$K \times L$ measurement matrix; see (2)
$\boldsymbol{\eta}_{\mathbf{K},\mathbf{L}}$	$K \times L$ additive noise matrix; see below (2)
$\mathcal{C}^k_\beta$	set of all compactly supported C^k-smooth functions $f : \mathbb{R} \to \mathbb{C}$ with $\mathrm{supp}(f) \subset (-\pi, \pi)$ and β Fourier Decay
$\tilde{\mathcal{C}}^k_{a,\beta}$	set of all compactly supported C^k-smooth functions $f : \mathbb{R} \to \mathbb{C}$ with $\mathrm{supp}(f) \subseteq (-a, a)$ and β Fourier decay
$\hat{f}$	either suitably renormalized Fourier transform of a function f or Fourier series coefficients of $f\|_{[-\pi,\pi]}$ (see (9))
Introduced in Chapter 2	
$m(x)$	mask $\tilde{m}$ or 2π-periodic extension of $\tilde{m}$
$\mathbf{Z}$	matrix with noisless measurements; see (7)
$\boldsymbol{\eta}$	additive noise matrix with $\mathbf{Y} = \mathbf{Z} + \boldsymbol{\eta}$
$P_{\mathcal{A}}$	Fourier projection operator for a set $\mathcal{A} \subseteq \mathbb{Z}$; see (11)
$\mathcal{R} \coloneqq [r]_c$, $\mathcal{S} \coloneqq [s]_c$	for odd numbers r, s, and d with $r + s < d$
$\mathbf{T}$	matrix of measurements truncated by Fourier projection; see (12)
$\mathbf{x} \coloneqq (x_p)_{p\in\mathcal{D}}$	$x_p \coloneqq P_{\mathcal{S}} f\left(\frac{2\pi p}{d}\right)$
$\mathbf{y} \coloneqq (y_p)_{p\in\mathcal{D}}$,	$y_p \coloneqq P_{\mathcal{R}} m\left(\frac{2\pi p}{d}\right)$
$\mathbf{z} \coloneqq (z_p)_{p\in\mathcal{D}}$	$z_p = m\left(\frac{2\pi p}{d}\right)$
$\mathbf{T}'$	approximation of $\mathbf{T}$ depending on $\mathbf{z}$ instead of $\mathbf{y}$; see (15)
Introduced in Chapter 3	
$\mathbf{E}$	total error matrix, i.e. $\mathbf{E} \coloneqq \mathbf{Y} - \mathbf{T}' = (\mathbf{Z} - \mathbf{T}') + \boldsymbol{\eta}$
$\tilde{\mathbf{E}}$	$\tilde{\mathbf{E}} \coloneqq \mathbf{F_L} {\mathbf{E}_{\mathbf{K},\mathbf{L}}}^T {\mathbf{F_K}}^T$
$\tilde{\mathbf{T}}$	analog to $\tilde{\mathbf{E}}$ based on $\mathbf{T}'_{\mathbf{K},\mathbf{L}}$, see (16)
μ_1	mask-dependent constant under Assumption 1.2; see (22)
μ_2	mask-dependent constant under Assumption 1.3; see (36)
$\sigma_{\min}(\cdot)$	smallest singular value of a matrix
T_κ	restriction operator, $T_\kappa(\mathbf{M})_{ij} = M_{i,j}$ for $\|i-j\| \le \kappa - 1$ and 0 else
$R(\mathbf{M})$	$d \times (2\kappa - 1)$ matrix with entries defined by $R(M)_{i,j} = M_{i,i+j}$
H	Hermitianizing operator; see (30)
Λ	reshaping operator with $(\Lambda(M))_{i,j} = M_{i,j-i}$
$\mathbf{C}$	$(2\kappa - 1) \times (2s - 1)$ matrix for $s \le 2\kappa - 1$ with $C_{\omega,\ell} = \tilde{T}_{-\ell,\omega} \cdot (4\pi^2 d(\mathbf{F_d}(\widehat{\mathbf{z}} \circ S_{-\ell}\overline{\widehat{\mathbf{z}}}))_\omega)^{-1}$
$\mathbf{B}$, $\mathbf{D}$	matrices with $\mathbf{B} = \mathbf{C} + \mathbf{D}$ defined in (39)
$\mathbf{W}$	$(2\kappa - 1) \times s$ partial Fourier matrix with entries $W_{j,k} = (\mathbf{F_d})_{j,k}$
Introduced in Chapter 4	
$T_\gamma(\widehat{\mathbf{x}}\widehat{\mathbf{x}}^*) = \mathbf{A} + \mathbf{N}$	(see (44)) depending on Assumptions *Under Assumption 1.2:* $\gamma = \kappa$ and $\mathbf{A} \coloneqq H(\mathbf{X})$ and $\mathbf{N} \coloneqq H(\tilde{\mathbf{N}})$ with $\mathbf{X}$ and $\tilde{\mathbf{N}}$ defined in (27) and (28) *Under Assumption 1.3:* $\gamma = 2s - 1$ and $\mathbf{A} \coloneqq H(\Lambda(\mathbf{W}^\dagger \mathbf{C}))$ and $\mathbf{N} \coloneqq H(\Lambda(\mathbf{W}^\dagger \mathbf{D}))$ where $\mathbf{W}^\dagger$ is the pseudoinverse of $\mathbf{W}$
f_e	trigonometric polynomial approximating f; see (48)

As a result, the assumptions that the support of f is contained in $(-a, a)$ and that $a < \pi - b$ imply that

$$\int_{-\pi}^{\pi} f(x) \left(\tilde{m}\left(x - \frac{2\pi}{d}\ell\right) - m\left(x - \frac{2\pi}{d}\ell\right) \right) \mathrm{e}^{-\mathrm{i}x\omega} dx = 0$$

and so (8) follows.

For any C^2-smooth function $g : \mathbb{R} \to \mathbb{C}$, we will define

$$\widehat{g}(n) \coloneqq \frac{1}{2\pi} \int_{-\pi}^{\pi} g(x) \mathrm{e}^{-\mathrm{i}nx} dx \tag{9}$$

for all $n \in \mathbb{Z}$, and note that, if g is 2π-periodic, we may use Fourier series to write

$$g(x) = \sum_{n \in \mathbb{Z}} \widehat{g}(n) \mathrm{e}^{\mathrm{i}nx}. \tag{10}$$

We also note that, if g is not 2π-periodic, but its support is contained in $(-\pi, \pi)$, then (10) still holds for all $x \in (-\pi, \pi)$ since we may view $\{\widehat{g}(n)\}_{n \in \mathbb{Z}}$ as the Fourier coefficients of the periodized version of g. For any set $\mathcal{A} \subseteq \mathbb{Z}$, we define $P_{\mathcal{A}}$ to be the Fourier projection operator given by

$$P_{\mathcal{A}} g(x) \coloneqq \sum_{n \in \mathcal{A}} \widehat{g}(n) \mathrm{e}^{\mathrm{i}nx}. \tag{11}$$

Now, let r, s, and d be odd numbers with $r + s < d$. Let $\mathcal{R} \coloneqq [r]_c$, $\mathcal{S} \coloneqq [s]_c$, and $\mathcal{D} = [d]_c$ be the sets of r, s, and d consecutive integers centered at the origin. Let $\mathbf{T} \coloneqq (T_{\omega,\ell})_{\omega,\ell \in \mathcal{D}}$ denote the matrix of measurements obtained by replacing f with $P_{\mathcal{S}} f$ and m with $P_{\mathcal{R}} m$ in (8), i.e., the matrix whose entries are given by

$$T_{\omega,\ell} \coloneqq \left| \int_{-\pi}^{\pi} P_{\mathcal{S}} f(x) P_{\mathcal{R}} m\left(x - \frac{2\pi}{d}\ell\right) \mathrm{e}^{-\mathrm{i}x\omega} dx \right|^2. \tag{12}$$

If Assumption 1.2 holds, we will assume that $r > \rho + 1$ which implies $P_{\mathcal{R}} m(x) = m(x)$.

The following lemma provides a bound on the ℓ^∞-norm of the error matrix $\mathbf{Z} - \mathbf{T}$.

Lemma 2.1 *Let r, s, and d be odd numbers with $r + s < d$, and let $\tilde{m} : \mathbb{R} \to \mathbb{C}$ and $f : \mathbb{R} \to \mathbb{C}$ be C^k-smooth functions for some $k \geq 2$. Then, under Assumption 1.2, we have*

$$\|\mathbf{Z} - \mathbf{T}\|_\infty \leq C_{f,m} \left(\frac{1}{s}\right)^{k-1},$$

and, under Assumption 1.3, we have

$$\|\mathbf{Z} - \mathbf{T}\|_\infty \leq C_{f,m} \left(\left(\frac{1}{s}\right)^{k-1} + \left(\frac{1}{r}\right)^{k-1} \right).$$

In either case, $C_{f,m} \in \mathbb{R}^+$ is a generic constant that depends only on f, $\tilde{m}$, and k (and, in particular, is independent of s, r and d).

To prove Lemma 2.1, we need the following auxiliary lemma whose proof is classical. In particular, in the first inequality of Lemma 2.2, it is straightforward to check that one may choose C_g to be $\|g\|_{A(T)} \coloneqq \sum_{\omega\in\mathbb{Z}} |\hat{g}(\omega)|$, which is finite since Dirichlet's theorem implies that the Fourier series of a C^1 function is absolutely summable. The second inequality follows by verifying that $|\hat{g}(\omega)| \leq \|g^{(k)}\|_1 \omega^{-k}$ and summing over $\omega \geq (n+1)/2$. We also note that Lemma 2.2 can be applied both to 2π-periodic functions and to functions whose support is contained in $(-\pi, \pi)$.

Lemma 2.2 *Let $k \geq 2$, and let $g : \mathbb{R} \to \mathbb{C}$ be a C^k-smooth function such that (10) holds for all $x \in (-\pi, \pi)$. Let $n \geq 3$ be an odd number, let $\mathcal{N} \coloneqq [n]_c$, and let $\mathcal{A}$ be any subset of $\mathbb{Z}$. Then, there exists a constant depending only on g and k such that*

$$\|P_{\mathcal{A}} g\|_{L^\infty([-\pi,\pi])} \leq C_g \quad \text{and} \quad \|g - P_{\mathcal{N}} g\|_{L^\infty([-\pi,\pi])} \leq C_g \left(\frac{1}{n}\right)^{k-1},$$

where $P_{\mathcal{A}}$ and $P_{\mathcal{N}}$ are the Fourier projection operators defined as in (11).

The Proof of Lemma 2.1 We note that the measurements given in (8) and (12) may be written as

$$Z_{\omega,\ell} = |M_{\omega,\ell}|^2 \quad \text{and} \quad T_{\omega,\ell} = |U_{\omega,\ell}|^2,$$

where

$$M_{\omega,\ell} \coloneqq \int_{-\pi}^{\pi} f(x) m\left(x - \frac{2\pi}{d}\ell\right) \mathrm{e}^{-\mathrm{i}x\omega} dx \quad \text{and}$$
$$U_{\omega,\ell} \coloneqq \int_{-\pi}^{\pi} P_{\mathcal{S}} f(x) P_{\mathcal{R}} m\left(x - \frac{2\pi}{d}\ell\right) \mathrm{e}^{-\mathrm{i}x\omega} dx.$$

Lemma 2.2 implies

$$\|P_{\mathcal{R}} m\|_{L^\infty([-\pi,\pi])} \leq C_m \quad \text{and} \quad \|P_{\mathcal{S}} f\|_{L^\infty([-\pi,\pi])} \leq C_f.$$

Therefore,

$$|U_{\omega,\ell}| \leq 2\pi \|P_{\mathcal{R}} m\|_{L^\infty([-\pi,\pi])} \|P_{\mathcal{S}} f\|_{L^\infty([-\pi,\pi])} \leq C_{f,m}.$$

Next, letting $\tilde{\ell} = 2\pi\ell/d$, we note that

$$M_{\omega,\ell} - U_{\omega,\ell} = \int_{-\pi}^{\pi} \big(f(x) - P_{\mathcal{S}} f(x)\big) m(x - \tilde{\ell}) \mathrm{e}^{-\mathrm{i}\omega x} dx +$$
$$\int_{-\pi}^{\pi} P_{\mathcal{S}} f(x) \Big(m(x - \tilde{\ell}) - P_{\mathcal{R}} m(x - \tilde{\ell})\Big) \mathrm{e}^{-\mathrm{i}\omega x} dx.$$

Therefore, by Lemma 2.2 and the triangle inequality, we get

$$|M_{\omega,\ell} - U_{\omega,\ell}| \leq C_{f,m} \left(\left(\frac{1}{s}\right)^{k-1} + \|m - P_{\mathcal{R}} m\|_{L^\infty([-\pi,\pi])} \right).$$

Thus, we may use the difference of squares formula to see

$$|Z_{\omega,\ell} - T_{\omega,\ell}| = (|M_{\omega,\ell}| + |U_{\omega,\ell}|)||M_{\omega,\ell}| - |U_{\omega,\ell}||$$

$$\begin{aligned}
&\leq (2|U_{\omega,\ell}| + |M_{\omega,\ell} - U_{\omega,\ell}|)|M_{\omega,\ell} - U_{\omega,\ell}| \\
&\leq C_{f,m}\left(1 + \left(\frac{1}{s}\right)^{k-1} + \|m - P_{\mathcal{R}}m\|_{L^\infty([-\pi,\pi])}\right) \cdot \\
&\qquad\qquad \left(\left(\frac{1}{s}\right)^{k-1} + \|m - P_{\mathcal{R}}m\|_{L^\infty([-\pi,\pi])}\right).
\end{aligned}$$

Under Assumption 1.2, we have $\|m - P_{\mathcal{R}}m\|_{L^\infty([-\pi,\pi])} = 0$, and thus,

$$|Z_{\omega,\ell} - T_{\omega,\ell}| \leq C_{f,m}\left(1 + \left(\frac{1}{s}\right)^{k-1}\right)\left(\frac{1}{s}\right)^{k-1} \leq C_{f,m}\left(\frac{1}{s}\right)^{k-1}.$$

Likewise, under Assumption 1.3, Lemma 2.2 implies $\|m - P_{\mathcal{R}}m\|_{L^\infty([-\pi,\pi])} \leq C_m\left(\frac{1}{r}\right)^{k-1}$, and so

$$\begin{aligned}
|Z_{\omega,\ell} - T_{\omega,\ell}| &\leq C_{f,m}\left(1 + \left(\frac{1}{s}\right)^{k-1} + \left(\frac{1}{r}\right)^{k-1}\right)\left(\left(\frac{1}{s}\right)^{k-1} + \left(\frac{1}{r}\right)^{k-1}\right) \\
&\leq C_{f,m}\left(\left(\frac{1}{s}\right)^{k-1} + \left(\frac{1}{r}\right)^{k-1}\right).
\end{aligned}$$

□

Algorithms 1 and 2 rely on discretizing the integrals used in the definitions of our measurements. Towards this end, we define three vectors $\mathbf{x} \coloneqq (x_p)_{p\in\mathcal{D}}$, $\mathbf{y} \coloneqq (y_p)_{p\in\mathcal{D}}$, and $\mathbf{z} \coloneqq (z_p)_{p\in\mathcal{D}}$ by

$$x_p \coloneqq P_{\mathcal{S}}f\left(\frac{2\pi p}{d}\right), \quad y_p \coloneqq P_{\mathcal{R}}m\left(\frac{2\pi p}{d}\right), \quad \text{and} \quad z_p = m\left(\frac{2\pi p}{d}\right). \tag{13}$$

We note that under Assumption 1.2, we have $P_{\mathcal{R}}m(x) = m(x)$ and therefore $\mathbf{y} = \mathbf{z}$. Under Assumption 1.3, we have that $\mathrm{supp}(m) \cap [-\pi,\pi] \subseteq (-b,b)$. Therefore, $\mathrm{supp}(\mathbf{z}) \subseteq [\delta+1]_c$, where $\delta \coloneqq \lfloor \frac{b}{\pi}d \rfloor$. The following lemma shows that the integral used in the definition of $\mathbf{T}$ can be rewritten as a discrete sum. Please see Appendix A for a proof.

Lemma 2.3 *Let $\mathbf{x} = (x_p)_{p\in\mathcal{D}}$ and $\mathbf{y} = (y_p)_{p\in\mathcal{D}}$ be defined as in (13). Then, for all $\omega \in \mathcal{D}$, $\ell \in \mathbb{Z}$, and $\tilde{\ell} = \frac{2\pi\ell}{d}$, we have that*

$$\int_{-\pi}^{\pi} P_{\mathcal{S}}f(x)P_{\mathcal{R}}m(x - \tilde{\ell})\mathbb{e}^{-\mathbb{i}x\omega}dx = \frac{2\pi}{d}\sum_{p\in\mathcal{D}} x_p y_{p-\ell}\mathbb{e}^{-2\pi\mathbb{i}\omega p/d},$$

and as a consequence,

$$T_{\omega,\ell} = \frac{4\pi^2}{d^2}\left|\sum_{p\in\mathcal{D}} x_p y_{p-\ell}\mathbb{e}^{-2\pi\mathbb{i}\omega p/d}\right|^2. \tag{14}$$

The matrix $\mathbf{T}$ depends on the vector $\mathbf{y}$ which is obtained by sampling the trigonometric polynomial $P_{\mathcal{R}}m$. By construction, $\mathbf{y}$ is not compactly supported, i.e., its nonzero entries are not contained in interval which is short

relative to the length of the vector (even under Assumption 1.3). In Section 3, we will apply a Wigner Deconvolution method based on [8] to invert our discretized measurements. In order to do this, we will need to use the vector $\mathbf{z}$ which is obtained by subsampling m rather than $P_{\mathcal{R}}m$. (By construction, $\mathbf{z}$ will be compactly supported under Assumption 1.3, and under Assumption 1.2, we have $\mathbf{y} = \mathbf{z}$ and so this makes no difference.) This motivates the following lemma which shows that $\mathbf{T}$ is well-approximated by the matrix $\mathbf{T}' = (T'_{\omega,\ell})_{\omega,\ell\in\mathcal{D}}$ obtained by replacing $\mathbf{y}$ with $\mathbf{z}$ in (14), i.e.,

$$T'_{\omega,\ell} = \frac{4\pi^2}{d^2}\left|\sum_{p\in\mathcal{D}} x_p z_{p-\ell} \mathbb{e}^{-2\pi \mathbb{i}\omega p/d}\right|^2. \tag{15}$$

Lemma 2.4 *Let* $\mathbf{T}$ *and* $\mathbf{T}'$ *be the matrices defined in* (12) *and* (15)*. Then, under Assumption 1.2, we have*

$$\|\mathbf{T} - \mathbf{T}'\|_\infty = 0,$$

and under Assumption 1.3,

$$\|\mathbf{T} - \mathbf{T}'\|_\infty \leq C_{f,m}\left(\frac{1}{r}\right)^{k-1}.$$

Proof Under Assumption 1.2, we have $\mathbf{y} = \mathbf{z}$. Thus by (14) and (15) we have $\mathbf{T} = \mathbf{T}'$ and therefore the first claim is immediate. To prove the second claim, we will assume Assumption 1.3 holds and use arguments similar to those used in the proof of Lemma 2.1. Let

$$U_{\omega,\ell} = \frac{2\pi}{d}\sum_{p\in\mathcal{D}} x_p y_{p-\ell} \mathbb{e}^{-2\pi \mathbb{i}\omega p/d} \quad \text{and} \quad U'_{\omega,\ell} = \frac{2\pi}{d}\sum_{p\in\mathcal{D}} x_p z_{p-\ell} \mathbb{e}^{-2\pi \mathbb{i}\omega p/d}.$$

Then by Lemma 2.3 we have

$$T_{\omega,\ell} = |U_{\omega,\ell}|^2 \quad \text{and} \quad T'_{\omega,\ell} = |U'_{\omega,\ell}|^2.$$

By Lemma 2.2 and the fact that m is a continuous periodic function, we see

$$\begin{aligned}
\|\mathbf{x}\|_\infty &\leq \|P_{\mathcal{B}}f\|_{L^\infty([-\pi,\pi])} \leq C_f,\\
\|\mathbf{y}\|_\infty &\leq \|P_{\mathcal{R}}m\|_{L^\infty([-\pi,\pi])} \leq C_m, \quad \text{and}\\
\|\mathbf{z}\|_\infty &\leq \|m\|_{L^\infty([-\pi,\pi])} \leq C_m.
\end{aligned}$$

Therefore,

$$|U_{\omega,\ell}| + |U'_{\omega,\ell}| \leq C_{f,m}.$$

To bound $|U_{\omega,\ell} - U'_{\omega,\ell}|$, we may again apply Lemma 2.2, to see

$$|U_{\omega,\ell} - U'_{\omega,\ell}| \leq 2\pi\|\mathbf{x}\|_\infty\|\mathbf{y} - \mathbf{z}\|_\infty \leq C_f\|m - P_{\mathcal{R}}m\|_{L^\infty([-\pi,\pi])} \leq C_{f,m}\left(\frac{1}{r}\right)^{k-1}.$$

Therefore, by the same reasoning as in the proof of Lemma 2.1, we have

$$|T_{\omega,\ell} - T'_{\omega,\ell}| \leq (|U_{\omega,\ell}| + |U'_{\omega,\ell}|)(|U_{\omega,\ell} - U'_{\omega,\ell}|) \leq C_{f,m}\left(\frac{1}{r}\right)^{k-1}.$$

□

3 Wigner Deconvolution

In this section, we will use a Wigner Deconvolution method based on [8] to recover $\mathbf{x}$ from the matrix $\mathbf{T}'$ defined in (15). For the sake of exposition, we briefly outline this method as used in the discrete setting in [8] in the simple case where there is no noise and no subsampling, i.e., $\eta_{\omega,\ell} = 0$ and $K = L = d$. Under these settings, the measurements considered in [8] took the form

$$Y_{k,\ell} = |\langle S_\ell \mathbf{m_k}, \mathbf{x}\rangle|^2,$$

for $k, \ell \in \mathcal{D}$ where the $\mathbf{m_k}$ are a sequence of measurement masks each of which are obtained as modulations of a single base mask, i.e., $(\mathbf{m_k})_j = \mathbb{e}^{2\pi \mathbb{i} jk/d}\mathbf{m}_j$. Given this setup, one may compute (see Lemma 7 of [8][3])

$$Y_{k,\ell} = d^3(\mathbf{F_d}(\widehat{\mathbf{x}} \circ S_{-k}\overline{\widehat{\mathbf{x}}}))_\ell(\mathbf{F_d}(\widehat{\mathbf{m}} \circ S_k\overline{\widehat{\mathbf{m}}}))_\ell,$$

where $\widehat{\mathbf{x}} \coloneqq \mathbf{F_d}\mathbf{x}$ and $\widehat{\mathbf{m}} \coloneqq \mathbf{F_d}\mathbf{m}$ are the discrete Fourier transforms of $\mathbf{x}$ and $\mathbf{m}$. Therefore, under proper assumptions on $\mathbf{m}$ we have

$$(\mathbf{F_d}(\widehat{\mathbf{x}} \circ S_{-k}\overline{\widehat{\mathbf{x}}}))_\ell = \frac{Y_{k,\ell}}{d^3(\mathbf{F_d}(\widehat{\mathbf{m}} \circ S_k\overline{\widehat{\mathbf{m}}}))_\ell}.$$

Taking the inverse Fourier transform, we may compute $\widehat{\mathbf{x}} \circ S_{-k}\overline{\widehat{\mathbf{x}}}$ for all k. Therefore, we have recovered the Fourier autocorrelation matrix $\widehat{\mathbf{x}}\overline{\widehat{\mathbf{x}}}^*$ since each $\widehat{\mathbf{x}} \circ S_{-k}\overline{\widehat{\mathbf{x}}}$ is a diagonal band of the $\widehat{\mathbf{x}}\overline{\widehat{\mathbf{x}}}^*$. Noting that

$$(\widehat{\mathbf{x}}\overline{\widehat{\mathbf{x}}}^*)_{i,j} = \widehat{x}_i\overline{\widehat{x}_j},$$

we observe that the magnitudes of $\widehat{\mathbf{x}}$, $|\widehat{x}_i|$, are the square roots of the diagonal entries of $\widehat{\mathbf{x}}\overline{\widehat{\mathbf{x}}}^*$. Moreover, we may compute the phase differences of $\widehat{\mathbf{x}}$, $\mathrm{Arg}(\widehat{x}_i) - \mathrm{Arg}(\widehat{x}_j)$ from the off-diagonal entries since $\mathrm{Arg}(\widehat{x}_i\overline{\widehat{x}_j}) = \mathrm{Arg}(\widehat{x}_i) - \mathrm{Arg}(\widehat{x}_j)$. Since we only aim to recover $\mathbf{x}$ up to a global phase, we may assume$\mathrm{Arg}(\widehat{x}_0) = 0$, and therefore we have all the information we need in order to reconstruct $\widehat{\mathbf{x}}$. Finally, we may then solve for $\mathbf{x}$ via Fourier inversion.

Our method is based on taking the ideas discussed above and adapting them to our more complicated setting, carefully accounted for measurement noise, discretization error, and computational difficulties introduced from subsampling. In order to do this, we let $\mathbf{E}$ be the total error matrix defined by

$$\mathbf{E} \coloneqq \mathbf{Y} - \mathbf{T}'.$$

We note that $\mathbf{E}$ can be decomposed by

$$\mathbf{E} = (\mathbf{Z} - \mathbf{T}') + \boldsymbol{\eta},$$

[3] [8] used a different normalization of the Fourier transform than we use here, so their Lemma 7 will have a different power of d.

where $(\mathbf{Z} - \mathbf{T}')$ is the error due to discretization and $\boldsymbol{\eta}$ is measurement noise. Let K and L divide d. Let $\mathbf{E}_{\mathbf{K},\mathbf{L}}$ and $\mathbf{T}'_{\mathbf{K},\mathbf{L}}$ be the $K \times L$ matrices obtained by subsampling the columns of $\mathbf{E}$ and $\mathbf{T}'$ as in (4), and let let $\boldsymbol{\eta}_{\mathbf{K},\mathbf{L}}$ be the $K \times L$ matrix of noise entries on the sampled measurements. Similarly to [8], we introduce the quantities $\tilde{\mathbf{E}}$ and $\tilde{\mathbf{T}}$ defined by

$$\tilde{\mathbf{E}} \coloneqq \mathbf{F}_{\mathbf{L}} \mathbf{E}_{\mathbf{K},\mathbf{L}}{}^T \mathbf{F}_{\mathbf{K}}{}^T \quad \text{and} \quad \tilde{\mathbf{T}} \coloneqq \mathbf{F}_{\mathbf{L}} (\mathbf{T}'_{\mathbf{K},\mathbf{L}})^T \mathbf{F}_{\mathbf{K}}{}^T. \tag{16}$$

Since $\sqrt{L}\mathbf{F}_{\mathbf{L}}$ and $\sqrt{K}\mathbf{F}_{\mathbf{K}}$ are unitary, we have

$$\|\tilde{\mathbf{E}}\|_F = \|\mathbf{F}_{\mathbf{L}} \mathbf{E}_{\mathbf{K},\mathbf{L}}{}^T \mathbf{F}_{\mathbf{K}}{}^T\|_F \leq \frac{1}{\sqrt{KL}} \|\mathbf{E}_{\mathbf{K},\mathbf{L}}\|_F \leq \|\mathbf{Z} - \mathbf{T}'\|_\infty + \frac{1}{\sqrt{KL}} \|\boldsymbol{\eta}_{\mathbf{K},\mathbf{L}}\|_F.$$

Therefore, Lemmas 2.1 and 2.4 imply that under Assumption 1.2 we have

$$\|\tilde{\mathbf{E}}\|_F \leq C_{f,m} \left(\frac{1}{s}\right)^{k-1} + \frac{1}{\sqrt{KL}} \|\boldsymbol{\eta}_{\mathbf{K},\mathbf{L}}\|_F, \tag{17}$$

and that under Assumption 1.3 we have

$$\|\tilde{\mathbf{E}}\|_F \leq C_{f,m} \left(\left(\frac{1}{s}\right)^{k-1} + \left(\frac{1}{r}\right)^{k-1} \right) + \frac{1}{\sqrt{KL}} \|\boldsymbol{\eta}_{\mathbf{K},\mathbf{L}}\|_F. \tag{18}$$

It follows from Theorem 4 of [8] (restated in Appendix E as Theorem E.1) that

$$\tilde{T}_{\ell,\omega} = 4\pi^2 d \sum_{q \in \left[\frac{d}{L}\right]_c} \sum_{p \in \left[\frac{d}{K}\right]_c} \left(\mathbf{F}_{\mathbf{d}} \left(\widehat{\mathbf{x}} \circ S_{qL-\ell} \overline{\widehat{\mathbf{x}}}\right)\right)_{\omega - pK} \left(\mathbf{F}_{\mathbf{d}} \left(\widehat{\mathbf{z}} \circ S_{\ell - qL} \overline{\widehat{\mathbf{z}}}\right)\right)_{\omega - pK} + \tilde{E}_{\ell,\omega} \tag{19}$$

$$= \frac{4\pi^2}{d} \sum_{q \in \left[\frac{d}{L}\right]_c} \sum_{p \in \left[\frac{d}{K}\right]_c} \left(\mathbf{F}_{\mathbf{d}} \left(\mathbf{x} \circ S_{\omega - pK} \overline{\mathbf{x}}\right)\right)_{\ell - qL} \left(\mathbf{F}_{\mathbf{d}} \left(\mathbf{z} \circ S_{\omega - pK} \overline{\mathbf{z}}\right)\right)_{qL - \ell} + \tilde{E}_{\ell,\omega}, \tag{20}$$

where, as noted in Section 1.2, $\circ$ denotes the componentwise multiplication product and S denotes the circular shift operator defined as in (3). In Sections 3.1 and 3.2, we will be able to use (19) and (20) to recover a portion of the Fourier autocorrelation matrix $\widehat{\mathbf{x}}\widehat{\mathbf{x}}^*$. (Note that [8] uses a different normalization of the discrete Fourier transform and consequently (19) and (20) have different powers of d than the corresponding equations there.)

3.1 Wigner Deconvolution Under Assumption 1.2

In this subsection, we will assume our mask $\tilde{m}(x)$ satisfies Assumption 1.2, i.e., that it is a trigonometric polynomial with at most ρ nonzero coefficients

for some $\rho \leq r-1$. We also assume that $K = d$, that L divides d, and that $L = \rho + \kappa$ for some $2 \leq \kappa \leq \rho$.

Since $K = d$, equation (19) simplifies to

$$\tilde{T}_{\ell,\omega} = 4\pi^2 d \sum_{q \in \left[\frac{d}{L}\right]_c} \left(\mathbf{F_d}\left(\widehat{\mathbf{x}} \circ S_{qL-\ell}\overline{\widehat{\mathbf{x}}}\right)\right)_\omega \left(\mathbf{F_d}\left(\widehat{\mathbf{z}} \circ S_{\ell-qL}\overline{\widehat{\mathbf{z}}}\right)\right)_\omega + \tilde{E}_{\ell,\omega}.$$

To further simplify this expression, we use the following lemma.

Lemma 3.1 *Assume the mask $\tilde{m}(x)$ satisfies Assumption 1.2, that $K = d$, that L divides d, and that $L = \rho + \kappa$ for some $2 \leq \kappa \leq \rho$. Then, if $1 - \kappa \leq \ell \leq \kappa - 1$ and $q \in \left[\frac{d}{L}\right]_c$, $q \neq 0$, we have*

$$\widehat{\mathbf{z}} \circ S_{\ell-qL}\overline{\widehat{\mathbf{z}}} = 0.$$

Proof Since $\tilde{m}(x)$ satisfies Assumption 1.2, and $\mathbf{z}$ is defined as in (13), we have $\mathrm{supp}(\widehat{\mathbf{z}}) \subseteq [\rho+1]_c$. Therefore, it suffices to show that for $q \in \left[\frac{d}{L}\right]_c$, $q \neq 0$, we have $\rho + 1 \leq |\ell - qL| \leq d - \rho - 1$. When $q > 0$, we have $|\ell - qL| = qL - \ell$ since $\ell < \kappa < L$. Thus we see

$$|\ell - qL| = qL - \ell \geq L - (\kappa - 1) = \rho + 1,$$

and

$$|\ell - qL| = qL - \ell \leq \frac{\frac{d}{L} - 1}{2} L - (1 - \kappa) = \frac{d}{2} - \frac{\rho - \kappa}{2} - 1 \leq \frac{d}{2} - 1 \leq d - \rho - 1,$$

where in the last line we used the fact that $\rho \leq d/2$ by Assumption 1.2. The case where $q < 0$ is similar. □

Lemma 3.1 implies that if $1 - \kappa \leq \ell \leq \kappa - 1$, we have

$$\widehat{\mathbf{z}} \circ S_{\ell-qL}\overline{\widehat{\mathbf{z}}} = 0$$

except for when $q = 0$. Thus,

$$\tilde{T}_{\ell,\omega} = 4\pi^2 d \left(\mathbf{F_d}\left(\widehat{\mathbf{x}} \circ S_{-\ell}\overline{\widehat{\mathbf{x}}}\right)\right)_\omega \left(\mathbf{F_d}\left(\widehat{\mathbf{z}} \circ S_{\ell}\overline{\widehat{\mathbf{z}}}\right)\right)_\omega + \tilde{E}_{\ell,\omega} \quad \text{for all } vert\ell| \leq \kappa - 1. \tag{21}$$

In order use (21) to solve for $\left(\mathbf{F_d}\left(\widehat{\mathbf{x}} \circ S_{-\ell}\overline{\widehat{\mathbf{x}}}\right)\right)_\omega$, we must divide by $\left(\mathbf{F_d}\left(\widehat{\mathbf{z}} \circ S_{\ell}\overline{\widehat{\mathbf{z}}}\right)\right)_\omega$. This motivates us to introduce a mask-dependent constant defined by

$$\mu_1 := \min_{|p| \leq \kappa - 1, q \in \mathcal{D}} \left| \left(\mathbf{F_d}\left(\widehat{\mathbf{z}} \circ S_p\overline{\widehat{\mathbf{z}}}\right)\right)_q \right|. \tag{22}$$

Proposition 3.2 shows that it is relatively simple to construct a trigonometric polynomial $\tilde{m}(x)$ such that μ_1 is strictly positive. For a proof, please see Appendix B.

Proposition 3.2 *Assume that $\tilde{m}$ satisfies Assumption 1.2. Further assume*

$$\left|\widehat{m}\left(-\frac{\rho}{2}\right)\right| > 2\rho\left|\widehat{m}\left(-\frac{\rho}{2}+1\right)\right| \tag{23}$$

and

$$\left|\widehat{m}\left(-\frac{\rho}{2}+1\right)\right| \geq \left|\widehat{m}\left(-\frac{\rho}{2}+2\right)\right| \geq \ldots \geq \left|\widehat{m}\left(\frac{\rho}{2}\right)\right| > 0. \tag{24}$$

Then the mask-dependent constant μ_1 defined as in (22) satisfies

$$\mu_1 \geq \frac{1}{2d}\left|\widehat{m}\left(-\frac{\rho}{2}\right)\right|\left|\widehat{m}\left(-\frac{\rho}{2}+\kappa-1\right)\right| > 0.$$

For the rest of this section, we will assume that μ_1 is non-zero. Therefore, we may make a change of variables $\ell \to -\ell$ in (21) to see that

$$\begin{aligned}\left(\mathbf{F_d}\left(\widehat{\mathbf{x}} \circ S_\ell \overline{\widehat{\mathbf{x}}}\right)\right)_\omega &= \frac{1}{4\pi^2 d}\left(\frac{\tilde{T}_{-\ell,\omega} - \tilde{E}_{-\ell,\omega}}{(\mathbf{F_d}(\widehat{\mathbf{z}} \circ S_{-\ell}\widehat{\mathbf{z}}))_\omega}\right) \\ &= \frac{1}{4\pi^2 d}\left(\frac{\tilde{T}_{-\ell,\omega}}{(\mathbf{F_d}(\widehat{\mathbf{z}} \circ S_{-\ell}\overline{\widehat{\mathbf{z}}}))_\omega}\right) - \frac{1}{4\pi^2 d}\left(\frac{\tilde{E}_{-\ell,\omega}}{(\mathbf{F_d}(\widehat{\mathbf{z}} \circ S_{-\ell}\overline{\widehat{\mathbf{z}}}))_\omega}\right)\end{aligned}$$

for all $1-\kappa \leq \ell \leq \kappa - 1$. Writing the above equation in column form, we have

$$\mathbf{F_d}\left(\widehat{\mathbf{x}} \circ S_\ell \overline{\widehat{\mathbf{x}}}\right) = \frac{1}{4\pi^2 d}\left(\frac{\tilde{\mathbf{T}}^T_{-\ell}}{\mathbf{F_d}(\widehat{\mathbf{z}} \circ S_{-\ell}\overline{\widehat{\mathbf{z}}})}\right) - \frac{1}{4\pi^2 d}\left(\frac{\tilde{\mathbf{E}}^T_{-\ell}}{\mathbf{F_d}(\widehat{\mathbf{z}} \circ S_{-\ell}\overline{\widehat{\mathbf{z}}})}\right)$$

and so

$$\widehat{\mathbf{x}} \circ S_\ell \overline{\widehat{\mathbf{x}}} = \frac{1}{4\pi^2 d}\mathbf{F_d}^{-1}\left(\frac{\tilde{\mathbf{T}}^T_{-\ell}}{\mathbf{F_d}(\widehat{\mathbf{z}} \circ S_{-\ell}\overline{\widehat{\mathbf{z}}}))}\right) - \frac{1}{4\pi^2 d}\mathbf{F_d}^{-1}\left(\frac{\tilde{\mathbf{E}}^T_{-\ell}}{\mathbf{F_d}(\widehat{\mathbf{z}} \circ S_{-\ell}\overline{\widehat{\mathbf{z}}}}\right), \tag{25}$$

where, as mentioned in Section 1, the division of vectors is defined componentwise and $\mathbf{M}_j$ denotes the j-th column of a matrix $\mathbf{M}$.

Let $T_\kappa : \mathbb{C}^{d\times d} \to \mathbb{C}^{d\times d}$ be the restriction operator defined for $\mathbf{M} \in \mathbb{C}^{d\times d}$ by

$$T_\kappa(\mathbf{M})_{ij} = \begin{cases} M_{i,j} & \text{if } |i-j| \leq \kappa - 1, \\ 0 & \text{otherwise.} \end{cases}$$

Then, we may rewrite (25) in matrix form as

$$T_\kappa(\widehat{\mathbf{x}}\widehat{\mathbf{x}}^*) = \mathbf{X} + \tilde{\mathbf{N}}, \tag{26}$$

where the matrices $\mathbf{X} = (X_{i,j})_{i,j\in\mathcal{D}}$ and $\tilde{\mathbf{N}} = (\tilde{N}_{i,j})_{i,j\in\mathcal{D}}$ have entries defined by

$$X_{i,j} = \begin{cases} \frac{1}{4\pi^2 d}\left(\mathbf{F_d}^{-1}\left(\frac{\tilde{\mathbf{T}}^T_{i-j}}{\mathbf{F_d}(\widehat{\mathbf{z}} \circ S_{i-j}\overline{\widehat{\mathbf{z}}})}\right)\right)_i & \text{if } |i-j| \leq \kappa - 1, \\ 0 & \text{otherwise,} \end{cases} \tag{27}$$

and

$$\tilde{N}_{i,j} = \begin{cases} \frac{-1}{4\pi^2 d}\left(\mathbf{F_d}^{-1}\left(\frac{\tilde{\mathbf{E}}_{i-j}^T}{\mathbf{F_d}(\widehat{\mathbf{z}}\circ S_{i-j}\overline{\widehat{\mathbf{z}}})}\right)\right)_i & \text{if } |i-j| \le \kappa - 1, \\ 0 & \text{otherwise.} \end{cases} \tag{28}$$

For a $d \times d$ matrix, $\mathbf{M} = (M_{i,j})_{i,j\in\mathcal{D}}$, let $R(\mathbf{M}) = (R(M)_{i,j})_{i\in\mathcal{D},j\in[2\kappa-1]_c}$ be the $d \times (2\kappa - 1)$ matrix with entries defined by

$$R(M)_{i,j} = M_{i,i+j}.$$

Note that the columns of $R(\mathbf{M})$ are the diagonal bands of $\mathbf{M}$ which are near the main diagonal, and that in particular, the middle column, column zero, is the main diagonal. Since $\tilde{\mathbf{N}}$ is a banded matrix whose nonzero terms are within κ of the main diagonal, we see

$$\|\tilde{\mathbf{N}}\|_F = \|R(\tilde{\mathbf{N}})\|_F.$$

Therefore, since $\frac{1}{\sqrt{d}}\mathbf{F_d}^{-1}$ is unitary, we may bound the ℓ^2-norm of the columns of $R(\tilde{\mathbf{N}})$ by

$$\begin{aligned} \|R(\tilde{\mathbf{N}})_j\|_2 &= \left\| \frac{1}{4\pi^2 d}\mathbf{F_d}^{-1}\left(\frac{\tilde{\mathbf{E}}_{-j}^T}{\mathbf{F_d}(\widehat{\mathbf{z}}\circ S_{-j}\overline{\widehat{\mathbf{z}}})}\right)\right\|_2 \\ &\le \frac{1}{4\pi^2 d^{1/2}}\left\|\frac{\tilde{\mathbf{E}}_{-j}^T}{\mathbf{F_d}(\widehat{\mathbf{z}}\circ S_{-j}\overline{\widehat{\mathbf{z}}})}\right\|_2 \\ &\le \frac{1}{4\pi^2 d^{1/2}\mu_1}\|\tilde{\mathbf{E}}_{-j}^T\|_2, \end{aligned}$$

where μ_1 is the mask-dependent constant defined in (22). Therefore, by (17) with $K = d$, we have

$$\|\tilde{\mathbf{N}}\|_F = \|R(\tilde{\mathbf{N}})\|_F \le C\frac{1}{d^{1/2}\mu_1}\|\tilde{\mathbf{E}}\|_F \le C_{f,m}\frac{1}{d^{1/2}\mu_1}\left(\left(\frac{1}{s}\right)^{k-1} + \frac{1}{\sqrt{dL}}\|\boldsymbol{\eta}_{\mathbf{d},\mathbf{L}}\|_F\right). \tag{29}$$

Let $H : \mathbb{C}^{d\times d} \to \mathbb{C}^{d\times d}$ be the Hermitianizing operator

$$H(\mathbf{M}) = \frac{\mathbf{M} + \mathbf{M}^*}{2}. \tag{30}$$

Since $T_\kappa(\mathbf{x}\mathbf{x}^*)$ is Hermitian, applying H to both sides of (26) yields

$$T_\kappa(\widehat{\mathbf{x}}\widehat{\mathbf{x}}^*) = \mathbf{A} + \mathbf{N}, \tag{31}$$

where

$$\mathbf{A} \coloneqq H(\mathbf{X}) \text{ and } \mathbf{N} \coloneqq H(\tilde{\mathbf{N}}). \tag{32}$$

We note that by (29) and the triangle inequality, we have

$$\|\mathbf{N}\|_F \leq \|\tilde{\mathbf{N}}\|_F \leq C_{f,m}\frac{1}{d^{1/2}\mu_1}\left(\left(\frac{1}{s}\right)^{k-1} + \frac{1}{\sqrt{dL}}\|\boldsymbol{\eta}_{\mathbf{d},\mathbf{L}}\|_F\right). \tag{33}$$

3.2 Wigner Deconvolution Under Assumption 1.3

In this subsection, we assume $f(x)$ and $\tilde{m}(x)$ satisfy Assumption 1.3, i.e., that $\mathrm{supp}(f) \subseteq (-a,a)$ and $\mathrm{supp}(\tilde{m}) \subseteq (-b,b)$ with $a+b<\pi$. Note that, by construction, this implies that the vector $\mathbf{z}$ defined in (13) satisfies $\mathrm{supp}(\mathbf{z}) \subseteq [\delta+1]_c$, where $\delta = \lfloor \frac{bd}{\pi} \rfloor$. We also assume that $L=d$, that K divides d and that $K = \delta + \kappa$ for some $2 \leq \kappa \leq \delta$. Furthermore, we let $s < 2\kappa - 1$.

Since $L=d$, equation (20) simplifies to

$$\tilde{T}_{\ell,\omega} = \frac{4\pi^2}{d}\sum_{p\in\left[\frac{d}{K}\right]_c}\left(\mathbf{F}_{\mathbf{d}}\left(\mathbf{x}\circ S_{\omega-pK}\overline{\mathbf{x}}\right)\right)_\ell\left(\mathbf{F}_{\mathbf{d}}\left(\mathbf{z}\circ S_{\omega-pK}\overline{\mathbf{z}}\right)\right)_{-\ell} + \tilde{E}_{\ell,\omega}.$$

Furthermore, if $|\omega| \leq \kappa - 1$, then by the same reasoning as in Lemma 11 and Remark 1 of [8], all terms in the above sum are zero except for the term corresponding to $p=0$. Therefore,

$$\tilde{T}_{\ell,\omega} = \frac{4\pi^2}{d}\left(\mathbf{F}_{\mathbf{d}}\left(\mathbf{x}\circ S_\omega\overline{\mathbf{x}}\right)\right)_\ell\left(\mathbf{F}_{\mathbf{d}}\left(\mathbf{z}\circ S_\omega\overline{\mathbf{z}}\right)\right)_{-\ell} + \tilde{E}_{\ell,\omega} \quad \text{for all } |\omega| \leq \kappa-1. \tag{34}$$

The following lemma is a restatement of Lemma 3 of [8], although we note that our result appears slightly different due to the fact that we use a different normalization of the discrete Fourier transform.

Lemma 3.3 *For all ℓ and ω, we have*

$$\left(\mathbf{F}_{\mathbf{d}}\left(\mathbf{x}\circ S_\omega\overline{\mathbf{x}}\right)\right)_\ell = d\mathrm{e}^{2\pi\mathrm{i}\omega\ell/d}\left(\mathbf{F}_{\mathbf{d}}\left(\widehat{\mathbf{x}}\circ S_{-\ell}\overline{\widehat{\mathbf{x}}}\right)\right)_\omega.$$

Applying Lemma 3.3 to (34), we see that

$$\tilde{T}_{\ell,\omega} = 4\pi^2 d\left(\mathbf{F}_{\mathbf{d}}\left(\widehat{\mathbf{x}}\circ S_{-\ell}\overline{\widehat{\mathbf{x}}}\right)\right)_\omega\left(\mathbf{F}_{\mathbf{d}}\left(\widehat{\mathbf{z}}\circ S_\ell\overline{\widehat{\mathbf{z}}}\right)\right)_\omega + \tilde{E}_{\ell,\omega} \tag{35}$$

for all $|\omega| \leq \kappa - 1$. In order to solve for $\left(\mathbf{F}_{\mathbf{d}}\left(\widehat{\mathbf{x}}\circ S_{-\ell}\overline{\widehat{\mathbf{x}}}\right)\right)_\omega$, we need to divide by $\left(\mathbf{F}_{\mathbf{d}}\left(\widehat{\mathbf{z}}\circ S_\ell\overline{\widehat{\mathbf{z}}}\right)\right)_\omega$. This motivates us to introduce a second mask-dependent constant given by

$$\mu_2 \coloneqq \min_{\omega\in[2\kappa-1]_c,\ell\in[2s-1]_c}\left|\left(\mathbf{F}_{\mathbf{d}}\left(\widehat{\mathbf{z}}\circ S_\ell\overline{\widehat{\mathbf{z}}}\right)\right)_\omega\right|. \tag{36}$$

Proposition 3.4 shows that, for any given d, it is relatively simple to construct a mask $\tilde{m}(x)$ such that μ_2 is strictly positive. For a proof please see Appendix B.

Proposition 3.4 *Assume that $\tilde{m}(x)$ satisfies Assumption 1.3. Let $\mathbf{z} = (z_p)_{p\in\mathcal{D}}$ be the vector defined as in (13) by $z_p = m\left(\frac{2\pi p}{d}\right)$, and let $\delta = \lfloor \frac{b}{\pi} d \rfloor$. Let $\tilde{\delta} \leq \delta + 1$ and assume that supp$(\mathbf{z}) = \{n, n+1, \ldots, n+\tilde{\delta}-1\}$ for some $\kappa \leq \tilde{\delta} \leq \delta + 1$. Further assume that*

$$|z_n| > 2\tilde{\delta}|z_{n+1}| \tag{37}$$

and that

$$|z_{n+1}| \geq |z_{n+2}| \geq \ldots |z_{n+\tilde{\delta}-1}| > 0. \tag{38}$$

Then the mask-dependent constant μ_2 defined in (36) satisfies

$$\mu_2 \geq \frac{1}{2d^2}|z_n||z_{n+\kappa-1}| > 0.$$

Remark 3.5 *Given any vector $\mathbf{z} = (z_p)_{p\in\mathcal{D}}$, one may construct, e.g., through spline interpolation, a function $\tilde{m}(x)$ such that $\tilde{m}\left(\frac{2\pi p}{d}\right) = z_p$ for all $p \in \mathcal{D}$.*

For the rest of this section, we will assume that μ_2 is not equal to zero. Therefore, we may make a change of variables $\ell \to -\ell$ in (35) to see that

$$\begin{aligned}\left(\mathbf{F_d}\left(\widehat{\mathbf{x}} \circ S_\ell \overline{\widehat{\mathbf{x}}}\right)\right)_\omega &= \frac{1}{4\pi^2 d}\left(\frac{\tilde{T}_{-\ell,\omega} - \tilde{E}_{-\ell,\omega}}{(\mathbf{F_d}(\widehat{\mathbf{z}} \circ S_{-\ell}\overline{\widehat{\mathbf{z}}}))_\omega}\right) \\ &= \frac{1}{4\pi^2 d}\left(\frac{\tilde{T}_{-\ell,\omega}}{(\mathbf{F_d}(\widehat{\mathbf{z}} \circ S_{-\ell}\overline{\widehat{\mathbf{z}}}))_\omega}\right) - \frac{1}{4\pi^2 d}\left(\frac{\tilde{E}_{-\ell,\omega}}{(\mathbf{F_d}(\widehat{\mathbf{z}} \circ S_{-\ell}\overline{\widehat{\mathbf{z}}}))_\omega}\right).\end{aligned}$$

Now, recall that $s \leq 2\kappa - 1$, and let $\mathbf{B} \coloneqq (B_{\omega,\ell}), \mathbf{C} \coloneqq (C_{\omega,\ell})$, and $\mathbf{D} \coloneqq (D_{\omega,\ell})$ be $(2\kappa-1) \times (2s-1)$ matrices with entries defined by

$$B_{\omega,\ell} = \left(\mathbf{F_d}\left(\widehat{\mathbf{x}} \circ S_\ell \overline{\widehat{\mathbf{x}}}\right)\right)_\omega, \quad C_{\omega,\ell} = \frac{1}{4\pi^2 d}\left(\frac{\tilde{T}_{-\ell,\omega}}{(\mathbf{F_d}(\widehat{\mathbf{z}} \circ S_{-\ell}\overline{\widehat{\mathbf{z}}}))_\omega}\right), \quad \text{and} \tag{39}$$

$$D_{\omega,\ell} = \frac{-1}{4\pi^2 d}\left(\frac{\tilde{E}_{-\ell,\omega}}{(\mathbf{F_d}(\widehat{\mathbf{z}} \circ S_{-\ell}\overline{\widehat{\mathbf{z}}}))_\omega}\right)$$

for $\omega \in [2\kappa-1]_c$ and $\ell \in [2s-1]_c$ so that

$$\mathbf{B} = \mathbf{C} + \mathbf{D}.$$

Note that

$$\|\mathbf{D}\|_F \leq \frac{1}{4\pi^2 d\mu_2}\|\tilde{\mathbf{E}}\|_F, \tag{40}$$

where μ_2 is the mask-dependent constant defined in (36).

Next observe that we may factor $\mathbf{B} = \mathbf{W}\mathbf{V}$, where $\mathbf{V} \coloneqq (V_{j,k})_{j\in\mathcal{S},k\in[2s-1]_c}$ is the $s \times (2s-1)$ matrix with entries defined by $V_{j,k} = (\widehat{\mathbf{x}} \circ S_k\overline{\widehat{\mathbf{x}}})_j$ and $\mathbf{W} \coloneqq (W_{j,k})_{j\in[2\kappa-1]_c,k\in\mathcal{S}}$ is the $(2\kappa-1)\times s$ partial Fourier matrix with entries $W_{j,k} = (\mathbf{F_d})_{j,k}$. Since $s \leq 2\kappa - 1$, we may let $\mathbf{W}^\dagger \coloneqq (\mathbf{W}^*\mathbf{W})^{-1}\mathbf{W}^*$ be the pseudoinverse of $\mathbf{W}$ and see

$$\mathbf{V} = \mathbf{W}^\dagger\mathbf{C} + \mathbf{W}^\dagger\mathbf{D}.$$

Now, let $\Lambda : \mathbb{C}^{s\times(2s-1)} \to \mathbb{C}^{d\times d}$ be the reshaping operator defined by

$$(\Lambda(M))_{i,j} = M_{i,j-i}.$$

Note that the columns of $\mathbf{M}$ are diagonal bands of $\Lambda(M)$ with the middle column on the main diagonal. By construction, we have $T_{2s-1}(\widehat{\mathbf{x}}\widehat{\mathbf{x}}^*) = \Lambda(\mathbf{V})$. Therefore, since $T_{2s-1}(\widehat{\mathbf{x}}\widehat{\mathbf{x}}^*)$ is Hermitian, we have

$$T_{2s-1}(\widehat{\mathbf{x}}\widehat{\mathbf{x}}^*) = H(\Lambda(\mathbf{V})),$$

where H is the Hermitianizing operator introduced in (30). Therefore,

$$T_{2s-1}(\widehat{\mathbf{x}}\widehat{\mathbf{x}}^*) = \mathbf{A} + \mathbf{N}, \tag{41}$$

where

$$\mathbf{A} \coloneqq H(\Lambda(\mathbf{W}^\dagger\mathbf{C})) \quad \text{and} \quad \mathbf{N} \coloneqq H(\Lambda(\mathbf{W}^\dagger\mathbf{D})). \tag{42}$$

Since H is contractive, (40) implies

$$\|\mathbf{N}\|_F \leq \|\Lambda(\mathbf{W}^\dagger\mathbf{D})\| = \|\mathbf{W}^\dagger\mathbf{D}\|_F \leq \frac{1}{\sigma_{\min}(\mathbf{W})}\|\mathbf{D}\|_F \leq \frac{1}{4\pi^2 d\mu_2\sigma_{\min}(\mathbf{W})}\|\tilde{\mathbf{E}}\|_F,$$

where $\sigma_{\min}(\mathbf{W})$ is the smallest singular value of $\mathbf{W}$. Combining this with (18) yields

$$\|\mathbf{N}\|_F \leq C_{f,m}\frac{1}{d\mu_2\sigma_{\min}(\mathbf{W})}\left(\left(\frac{1}{s}\right)^{k-1} + \left(\frac{1}{r}\right)^{k-1} + \frac{1}{\sqrt{Kd}}\|\boldsymbol{\eta}_{\mathbf{K},\mathbf{d}}\|_F\right). \tag{43}$$

4 Convergence Guarantees

In this section, we will provide convergence guarantees for Algorithms 1 and 2. Specifically, we will prove Theorem 4.1 which guarantees that we can reconstruct $f(x)$ from a noisy Fourier autocorrelation matrix. Corollaries 4.2 and 4.3, which guarantee the convergence of our algorithms, will then follow immediately from (31), (33), (41), and (43), which are proved in Section 3.

Algorithm 1 Signal Recovery with Trigonometric Polynomial Masks

Inputs

1. Trigonometric polynomial mask $\tilde{m}$ satisfying Assumption 1.2.
2. Matrix $\mathbf{Y} = (Y_{\omega,\ell})_{\omega\in\mathcal{D},\ell\in\mathcal{L}}$ of spectrogram measurements defined as in (2).

Steps

1. Define vector $\mathbf{z} = (z_p)_{p\in\mathcal{D}}$ by $z_p = \tilde{m}\left(\frac{2\pi p}{d}\right)$.
2. Let $\kappa = L - \rho$, and for $1 - \kappa \leq \ell \leq \kappa - 1$, estimate

$$\mathbf{F_d}\left(\widehat{\mathbf{x}} \circ S_\ell \overline{\widehat{\mathbf{x}}}\right) \approx \frac{1}{4\pi^2 L d^2}\left(\frac{(\mathbf{F_L}\mathbf{Y}^T\mathbf{F_d}^T)_{-\ell}}{\mathbf{F_d}(\widehat{\mathbf{z}} \circ S_{-\ell}\overline{\widehat{\mathbf{z}}})}\right).$$

3. Apply an inverse Fourier transform to estimate the vectors $\widehat{\mathbf{x}} \circ S_\ell \overline{\widehat{\mathbf{x}}}$.
4. Organize these vectors into a banded matrix $\mathbf{X} = (X_{i,j})_{i,j\in\mathcal{D}}$ described as in (27).
5. Hermitianize $\mathbf{X}$ to obtain the matrix $\mathbf{A} = (A_{i,j})_{i,j\in\mathcal{D}}$ as described in (32).
6. Estimate $|\widehat{f}(n)| \approx a_n = \sqrt{|A_{n,n}|}$.
7. For $n \in \mathcal{S} = [s]_c$, choose $\{n_\ell\}_{\ell=0}^{\zeta}$ according to Algorithm 3 (where $\zeta \leq \frac{d}{\beta}$ is as in Algorithm 3).
8. Approximate

$$\arg\left(\widehat{f}(n)\right) \approx \alpha_n = \sum_{\ell=0}^{\zeta-1} \arg\left(A_{n_{\ell+1},n_\ell}\right).$$

Output

An approximation of f given by

$$f_e(x) = \sum_{n\in\mathcal{S}} a_n \mathbb{e}^{\mathbb{i}\alpha_n}\mathbb{e}^{\mathbb{i}nx}.$$

For the rest of this section, we will assume that there exists $1 \leq \gamma \leq d$ such that

$$T_\gamma(\widehat{\mathbf{x}}\widehat{\mathbf{x}}^*) = \mathbf{A} + \mathbf{N}. \tag{44}$$

Here, $\mathbf{A} = (A_{i,j})_{i,j\in\mathcal{D}}$ is a known approximation of the partial Fourier autocorrelation matrix $T_\gamma(\widehat{\mathbf{x}}\widehat{\mathbf{x}}^*)$ and $\mathbf{N} \in \mathbb{C}^{d\times d}$ is an arbitrary noise matrix. We note that, under Assumption 1.2, equation (31) shows that (44) holds with $\gamma = \kappa$. Similarly, under Assumption 1.3, equation (41) shows that (44) holds with $\gamma = 2s - 1$. We also remark that (33) and (43) provide bounds on $\|\mathbf{N}\|_F$ in these cases. We will also assume for the remainder of this section that there exists $\beta < \gamma/2$ such that f belongs to the class of functions with β Fourier decay introduced in Definition 1.4.

Algorithm 2 Signal Recovery with Compactly Supported Masks

Inputs

1. Compactly supported mask $\tilde{m}$ satisfying Assumption 1.3.
2. Matrix $\mathbf{Y} = (Y_{\omega,\ell})_{\omega\in\mathcal{K},\ell\in\mathcal{D}}$ of spectrogram measurements defined as in (2).

Steps

1. Define vector $\mathbf{z} = (z_p)_{p\in\mathcal{D}}$ by $z_p = \tilde{m}\left(\frac{2\pi p}{d}\right)$.
2. Let $\kappa = K - \delta$, and for $1-\kappa \le \omega \le \kappa - 1, 1 - s \le \ell \le s-1$ estimate

$$\mathbf{F_d}\left(\widehat{\mathbf{x}} \circ S_\ell \overline{\widehat{\mathbf{x}}}\right) \approx \frac{1}{4\pi^2 K d^2}\left(\frac{(\mathbf{F_d}\mathbf{Y}^T\mathbf{F_K}^T)_{-\ell}}{(\mathbf{F_d}(\widehat{\mathbf{z}} \circ S_{-\ell}\overline{\widehat{\mathbf{z}}}))}\right).$$

3. Form the matrix $\mathbf{C}$ according to (39).
4. Compute $\mathbf{V} = \mathbf{W}^\dagger\mathbf{C}$, where $\mathbf{W} = ((\mathbf{F_d})_{j,k})_{j\in[2\kappa-1]_c,k\in\mathcal{S}}$ is the $(2\kappa-1)\times s$ partial Fourier matrix.
5. Apply reshaping operator Λ.
6. Hermitianize $\Lambda(\mathbf{V})$ to obtain the matrix $\mathbf{A} = (A_{i,j})_{i,j\in\mathcal{D}}$ as described in (42).
7. Estimate $|\widehat{f}(n)| \approx a_n = \sqrt{|A_{n,n}|}$.
8. For $n \in \mathcal{S} = [s]_c$, choose $\{n_\ell\}_{\ell=0}^{\zeta}$ according to Algorithm 3 (where $\zeta \le \frac{d}{\beta}$ is as in Algorithm 3).
9. Approximate

$$\arg\left(\widehat{f}(n)\right) \approx \alpha_n = \sum_{\ell=0}^{\zeta-1} \arg\left(A_{n_{\ell+1},n_\ell}\right).$$

Output

An approximation of f given by

$$f_e(x) = \sum_{n\in\mathcal{S}} a_n \mathbb{e}^{\mathbb{i}\alpha_n}\mathbb{e}^{\mathbb{i}nx}.$$

By construction, the discrete Fourier transform of the vector $\mathbf{x}$ defined in (13) satisfies

$$\widehat{x}_n = \widehat{f}(n) \text{ for all } n \in \mathcal{S},$$

and so the square magnitudes of the Fourier coefficients of f lie on the main diagonal of the matrix $T_\gamma(\widehat{\mathbf{x}}\widehat{\mathbf{x}}^*)$. Therefore, we view $a_n \coloneqq \sqrt{|A_{n,n}|}$ as an approximation of $|\widehat{x}_n|$. More specifically, Lemma 3 of [24] shows that

$$\left|a_n - |\widehat{f}(n)|\right|^2 \le 3\|\mathbf{N}\|_\infty. \tag{45}$$

Algorithm 3 Entry Selection

Inputs

1. Vector of amplitudes $\mathbf{a} = (a_n)_{n\in\mathcal{D}}, \quad a_n = \sqrt{|A_{n,n}|}$.
2. Entry $n \in \mathcal{S} = [s]_c$.

Steps

1. Choose $n_0 = \arg\max_{n\in\mathcal{S}} a_n$.
2. Let $\zeta = 0$.
3. While: $|n - n_\zeta| \geq \gamma$ (see (44)).
   If: $n > n_\zeta$, let $n_{\zeta+1} \leftarrow \arg\max_{n_\zeta+\gamma-\beta\leq m<n_\zeta+\gamma} a_m$.
   If: $n < n_\zeta$, let $n_{\zeta+1} \leftarrow \arg\max_{n_\zeta-\gamma<m\leq n_\zeta-\gamma+\beta} a_m$.
   $\zeta \leftarrow \zeta + 1$.
4. $n_\zeta \leftarrow n$.

Output

A sequence $\{n_\ell\}_{\ell=0}^{\zeta}$, $|n_{\ell+1} - n_\ell| < 2\beta$, $n_\zeta = n$, $\zeta \leq \frac{d}{\beta}$.

In addition to our estimate on the magnitudes of $\hat{f}(n)$, $|\hat{f}(n)| \approx a_n = \sqrt{A_{n,n}}$, we also need an estimate on the phase of each entry. In order to do this, we let $n_0 = \arg\max_{n\in\mathcal{S}} a_n$ and for $n \in \mathcal{D}$ we construct a sequence of indices $\{n_0, n_1, \ldots, n_\zeta = n\}$ such that $\zeta \leq \frac{d}{\beta}$ and each of the a_{n_ℓ} are as large as possible subject to the constraints that (i) $|n_{\ell+1} - n_\ell| \leq 2\beta$ and (ii) $|n_{\ell+1} - n| < |n_\ell - n|$. Full details on this construction are provided in Algorithm 3. We note that while superficially it appears that Algorithm 3 needs to be run repeatedly for every n, upon inspection, it is clear that it will select the same n_ℓ every time, except possibly for the last entry. Therefore, for computational savings, one may first compute sequences going from n_0 to $(d-1)/2$ and n_0 to $-(d-1)/2$. Then, one may use subsequences of these two longest sequences to contruct sequences from n_0 to any intermediate n's.

After constructing the sequence $\{n_0, \ldots, n_\zeta = n\}$, we then define

$$\alpha_n \coloneqq \sum_{l=0}^{\zeta-1} \arg\left(A_{n_{\ell+1},n_\ell}\right). \tag{46}$$

To understand this definition, we let

$$\theta_0 \coloneqq \arg(\widehat{f}(n_0)) \quad \text{and} \quad \tau_n \coloneqq \sum_{l=0}^{\zeta-1} \arg\left((\widehat{\mathbf{x}}\widehat{\mathbf{x}}^*)_{n_{\ell+1},n_\ell}\right). \tag{47}$$

By construction, $\tau_n = \arg\left(\widehat{f}(n)\right) - \theta_0$. Therefore

$$\mathrm{e}^{-\mathrm{i}\theta_0}\widehat{f}(n) = |\widehat{f}(n)|\mathrm{e}^{\mathrm{i}\tau_n}$$

for all $n \in \mathcal{S}$. (Note that n_0 does not depend on n.) Since $\mathbf{A}$ is a noisy approximation of (a portion of) $\widehat{\mathbf{x}}\widehat{\mathbf{x}}^*$, we intuitively view α_n as a noisy approximation of τ_n (up to a phase shift θ_0). Lemma 4.5 will show that this intuition is correct when $|\widehat{f}(n)|$ is sufficiently large. Therefore, in light of (45), we define a trigonometric polynomial, $f_e(x)$, which estimates $f(x)$ by

$$f_e(x) := \sum_{n\in\mathcal{S}} a_n \mathbb{e}^{\mathbb{i}\alpha_n} \mathbb{e}^{\mathbb{i}nx}. \tag{48}$$

The following theorem shows that $f_e(x)$ is a good approximation of $f(x)$.

Theorem 4.1 *Assume that $f(x)$ has β Fourier decay for some $\beta < \gamma/2$. For $n \in \mathcal{S}$, let α_n be defined as in (46), let $a_n = \sqrt{A_{n,n}}$, and let $f_e(x)$ be the trigonometric polynomial defined as in (48). Then,*

$$\min_{\theta\in[0,2\pi]} \|\mathbb{e}^{\mathbb{i}\theta} f - f_e\|^2_{L^2([-\pi,\pi])} \le C\, s \left(\frac{d}{\gamma}\right)^2 \|\mathbf{N}\|_\infty + C_f \left(\frac{1}{s}\right)^{2k-2}.$$

Before proving Theorem 4.1, we recall that $\gamma = \kappa$ under Assumption 1.2 and $\gamma = 2s-1$ under Assumption 1.3. Therefore, (33), (43), and the fact that $\|\mathbf{N}\|_\infty \le \|\mathbf{N}\|_F$, immediately lead to the following corollaries.

Corollary 4.2 (Convergence Guarantees for Algorithm 1) *Let $s+r<d$, let $K=d$, and let L divide d. Assume that $f(x)$ and $\tilde{m}(x)$ satisfy Assumption 1.2, that $\rho \le r-1$, and that $L = \rho+\kappa$ for some $2 \le \kappa \le \rho$. Then the trigonometric polynomial $f_e(x)$ output by Algorithm 1 satisfies*

$$\begin{aligned}&\min_{\theta\in[0,2\pi]} \|\mathbb{e}^{\mathbb{i}\theta} f - f_e\|^2_{L^2([-\pi,\pi])}\\ \le& C_{f,m}\left(\frac{sd^{3/2}}{\kappa^2\mu_1}\left(\left(\frac{1}{s}\right)^{k-1} + \frac{1}{\sqrt{dL}}\|\boldsymbol{\eta}_{\mathbf{d},\mathbf{L}}\|_F\right) + \left(\frac{1}{s}\right)^{2k-2}\right),\end{aligned}$$

where μ_1 is the mask-dependent constant defined in (22). Moreover, if $s > d/2$, then

$$\begin{aligned}&\min_{\theta\in[0,2\pi]} \|\mathbb{e}^{\mathbb{i}\theta} f - f_e\|^2_{L^2([-\pi,\pi])}\\ \le& C_{f,m}\left(\frac{1}{\kappa^2\mu_1}\left(\frac{1}{d}\right)^{k-7/2} + \frac{d^2}{\kappa^2 L^{1/2}\mu_1}\|\boldsymbol{\eta}_{\mathbf{d},\mathbf{L}}\|_F + \left(\frac{1}{d}\right)^{2k-2}\right).\end{aligned}$$

Corollary 4.3 (Convergence Guarantees for Algorithm 2) *Let $s+r<d$, let $L=d$, and let K divide d. Assume $f(x)$ and $\tilde{m}(x)$ satisfy Assumption 1.3 and let $\delta = \lfloor \frac{bd}{\pi} \rfloor$. Further, assume that $K = \delta+\kappa$ for some $2 \le \kappa \le \delta$ and that $s < 2\kappa - 1$. Then the trigonometric polynomial $f_e(x)$ output by Algorithm 2, satisfies*

$$\begin{aligned}&\min_{\theta\in[0,2\pi]} \|\mathbb{e}^{\mathbb{i}\theta} f - f_e\|^2_{L^2([-\pi,\pi])}\\ \le& C_{f,m}\left(\frac{d}{s\mu_2\sigma_{\min}(\mathbf{W})}\left(\left(\frac{1}{s}\right)^{k-1} + \left(\frac{1}{r}\right)^{k-1} + \frac{1}{\sqrt{Kd}}\|\boldsymbol{\eta}_{\mathbf{K},\mathbf{d}}\|_F\right) + \left(\frac{1}{s}\right)^{2k-2}\right),\end{aligned}$$

where μ_2 is the mask-dependent constant defined in (36). Moreover, if $s, r \geq \frac{db}{2\pi}$, then

$$\min_{\theta\in[0,2\pi]} \|\mathrm{e}^{\mathrm{i}\theta} f - f_e\|^2_{L^2([-\pi,\pi])}$$
$$\leq C_{f,m}\left(\frac{1}{\mu_2\sigma_{\min}(\mathbf{W})b^{k-1}d^k} + \frac{d^{1/2}}{K^{1/2}\mu_2\sigma_{\min}(\mathbf{W})}\|\boldsymbol{\eta}_{\mathbf{K},\mathbf{d}}\|_F + \left(\frac{1}{bd}\right)^{2k-2}\right).$$

In order to prove Theorem 4.1, we need the following lemma which provides us with an estimate of $\|\mathrm{e}^{-\mathrm{i}\theta_0}P_{\mathcal{S}}f - f_e\|_{L^2([-\pi,\pi])}$ as well as the uniform convergence of Fourier series.

Lemma 4.4 *Assume that $f(x)$ has β Fourier decay for some $\beta < \gamma/2$. For $n \in \mathcal{S}$, let α_n be defined as in (46), let $a_n = \sqrt{A_{n,n}}$, and let $f_e(x)$ be the trigonometric polynomial defined as in (48) by $f_e(x) = \sum_{n\in\mathcal{S}} a_n \mathrm{e}^{\mathrm{i}\alpha_n}\mathrm{e}^{\mathrm{i}nx}$. Then,*

$$\left\|\mathrm{e}^{-\mathrm{i}\theta_0}P_{\mathcal{S}}f - f_e\right\|^2_{L^2([-\pi,\pi])} \leq C\, s\left(\frac{d}{\gamma}\right)^2 \|\mathbf{N}\|_\infty.$$

In order to prove Lemma 4.4, we need the following lemma, which is a modification of [24, Lemma 4]. It shows that α_n is a good approximation of τ_n for all n such that $|\widehat{f}(n)|$ is sufficiently large. For a proof, please see Appendix C.

Lemma 4.5 *Suppose that f has β Fourier decay for some $\beta \leq \gamma/2$, and let L_f be the set of indices corresponding to large Fourier coefficients defined by*

$$L_f \coloneqq \{n \in \mathcal{S} : |\widehat{f}(n)|^2 \geq 48\|\mathbf{N}\|_\infty\}. \tag{49}$$

Let $n \in L_f$, and let τ_n and α_n be as in (46) and (47). Then

$$|\mathrm{e}^{\mathrm{i}\tau_n} - \mathrm{e}^{\mathrm{i}\alpha_n}| \leq \frac{4\pi d}{\gamma}\frac{\|\mathbf{N}\|_\infty}{|\widehat{f}(n)|^2}.$$

The Proof of Lemma 4.4 Recall that $\widehat{\mathbf{x}}_n = \widehat{f}(n)$ for all $n \in \mathcal{S}$, and let $\widehat{\mathbf{x}}_{|\mathcal{S}}$ be a vector of length s obtained by restricting $\widehat{\mathbf{x}}$ to indices in $\mathcal{S}$. Define vectors $\mathbf{u} = (u_n)_{n\in\mathcal{S}}$ and $\mathbf{v} = (v_n)_{n\in\mathcal{S}}$ by

$$u_n = a_n\mathrm{e}^{\mathrm{i}\alpha_n} \quad \text{and} \quad v_n = |\widehat{f}(n)|\mathrm{e}^{\mathrm{i}\alpha_n}.$$

By Parseval's identity, we see

$$\left\|\mathrm{e}^{-\mathrm{i}\theta_0}P_{\mathcal{S}}f(x) - \sum_{n\in\mathcal{S}} a_n\mathrm{e}^{\mathrm{i}\alpha_n}\mathrm{e}^{\mathrm{i}nx}\right\|_{L^2([-\pi,\pi])}$$
$$= \left\|\mathrm{e}^{-\mathrm{i}\theta_0}\sum_{n\in\mathcal{S}}\widehat{f}(n)\mathrm{e}^{\mathrm{i}nx} - \sum_{n\in\mathcal{S}} u_n\mathrm{e}^{\mathrm{i}nx}\right\|_{L^2([-\pi,\pi])}$$
$$\leq \sqrt{2\pi}\left\|\mathrm{e}^{-\mathrm{i}\theta_0}\widehat{\mathbf{x}}_{|\mathcal{S}} - \mathbf{u}\right\|_{\ell_2}$$

$$\begin{aligned}
&\leq \sqrt{2\pi}\left\| \mathrm{e}^{-\mathrm{i}\theta_0}\widehat{\mathbf{x}}_{|\mathcal{S}} - \mathbf{v}\right\|_{\ell_2} + \sqrt{2\pi}\|\mathbf{u}-\mathbf{v}\|_{\ell_2} \\
&=: I_1 + I_2.
\end{aligned}$$

To estimate I_2, we recall (45) and note

$$\begin{aligned}
I_2^2 &= 2\pi \sum_{n\in\mathcal{S}} |u_n - v_n|^2 \\
&= 2\pi \sum_{n\in\mathcal{S}} \left| a_n \mathrm{e}^{\mathrm{i}\alpha_n} - |\widehat{f}(n)| \mathrm{e}^{\mathrm{i}\alpha_n} \right|^2 \\
&= 2\pi \sum_{n\in\mathcal{S}} \left| a_n - |\widehat{x}_n| \right|^2 \\
&\leq 6\pi s \|\mathbf{N}\|_\infty. \qquad (50)
\end{aligned}$$

Using Lemma 4.5 and the fact that $|\mathrm{e}^{\mathrm{i}\tau_n} - \mathrm{e}^{\mathrm{i}\alpha_n}| \leq 2$, we have

$$\begin{aligned}
I_1^2 &= 2\pi \sum_{n\in\mathcal{S}} |\widehat{f}(n)|^2 |\mathrm{e}^{\mathrm{i}\tau_n} - \mathrm{e}^{\mathrm{i}\alpha_n}|^2 \\
&\leq C \sum_{n\in\mathcal{S}\setminus L_f} |\widehat{f}(n)|^2 + C \sum_{n\in L_f} \left(\frac{d}{\gamma}\right)^2 \|\mathbf{N}\|_\infty^2 \, |\widehat{f}(n)|^{-2} \\
&\leq C\, s\, \|\mathbf{N}\|_\infty + C \sum_{n\in L_f} \left(\frac{d}{\gamma}\right)^2 \|\mathbf{N}\|_\infty \\
&\leq C\, s \left(\frac{d}{\gamma}\right)^2 \|\mathbf{N}\|_\infty,
\end{aligned}$$

where L_f is the set of indices corresponding to large Fourier coefficients introduced in (49). Combining this with (50) yields

$$\left\| \mathrm{e}^{-\mathrm{i}\theta_0} P_{\mathcal{S}} f(x) - \sum_{n\in\mathcal{S}} a_n \mathrm{e}^{\mathrm{i}nx} \mathrm{e}^{\mathrm{i}\alpha_n} \right\|_{L^2([-\pi,\pi])}^2 \leq C\, s \left(\frac{d}{\gamma}\right)^2 \|\mathbf{N}\|_\infty$$

as desired. □

Theorem 4.1 now follows readily via Lemmas 2.2 and 4.5

The Proof of Theorem 4.1 For all $\theta \in [0, 2\pi]$, we have

$$\begin{aligned}
&\left\| \mathrm{e}^{\mathrm{i}\theta} f(x) - \sum_{n\in\mathcal{S}} a_n \mathrm{e}^{\mathrm{i}\alpha_n} \mathrm{e}^{\mathrm{i}nx} \right\|_{L^2([-\pi,\pi])} \\
\leq &\left\| \mathrm{e}^{\mathrm{i}\theta} f(x) - \mathrm{e}^{\mathrm{i}\theta} P_{\mathcal{S}} f(x) \right\|_{L^2([-\pi,\pi])} + \left\| \mathrm{e}^{\mathrm{i}\theta} P_{\mathcal{S}} f(x) - \sum_{n\in\mathcal{S}} a_n \mathrm{e}^{\mathrm{i}\alpha_n} \mathrm{e}^{\mathrm{i}nx} \right\|_{L^2([-\pi,\pi])} \\
= &\|f(x) - P_{\mathcal{S}} f(x)\|_{L^2([-\pi,\pi])} + \left\| \mathrm{e}^{-\mathrm{i}\theta} P_{\mathcal{S}} f(x) - \sum_{n\in\mathcal{S}} a_n \mathrm{e}^{\mathrm{i}\alpha_n} \mathrm{e}^{\mathrm{i}nx} \right\|_{L^2([-\pi,\pi])}.
\end{aligned}$$

Thus, letting $\theta_0 = \arg(\widehat{f}(n_0))$. Then we get

$$\begin{aligned}
&\min_{\theta\in[0,2\pi]} \left\| \mathrm{e}^{\mathrm{i}\theta} f(x) - \sum_{n\in\mathcal{S}} a_n \mathrm{e}^{\mathrm{i}\alpha_n} \mathrm{e}^{\mathrm{i}nx} \right\|_{L^2([-\pi,\pi])} \\
\leq &\|f(x) - P_{\mathcal{S}} f(x)\|_{L^2([-\pi,\pi])} + \left\| \mathrm{e}^{-\mathrm{i}\theta_0} P_{\mathcal{S}} f(x) - \sum_{n\in\mathcal{S}} a_n \mathrm{e}^{\mathrm{i}\alpha_n} \mathrm{e}^{\mathrm{i}nx} \right\|_{L^2([-\pi,\pi])}.
\end{aligned}$$

By Lemma 4.4, we know that

$$\left\| \mathbb{e}^{-\mathbb{i}\theta_0} P_{\mathcal{S}} f(x) - \sum_{n\in\mathcal{S}} a_n \mathbb{e}^{\mathbb{i}\alpha_n} \mathbb{e}^{\mathbb{i}nx} \right\|^2_{L^2([-\pi,\pi])} \leq C\, s \left(\frac{d}{\gamma}\right)^2 \|\mathbf{N}\|_\infty.$$

Therefore, we conclude by applying Lemma 2.2 to see

$$\|f - P_{\mathcal{S}} f\|^2_{L^2([-\pi,\pi])} \leq 2\pi \|f - P_{\mathcal{S}} f\|^2_{L^\infty([-\pi,\pi])} \leq C_f \left(\frac{1}{s}\right)^{2k-2}.$$

□

We will now finally prove Theorems 1.6 and 1.8.

Proof of Theorem 1.6 Apply Corollary 4.2 with $s = \lceil (d+1)/2 \rceil$ and $r = d - s - 1 \geq d/2 - 2$. The assumption that $d \geq 2\rho + 6$, implies that $\rho \leq r - 1$. Noting now that $\kappa \coloneqq L - \rho \geq 2$ and applying Proposition 3.2 for choices of $\tilde{m}$ satisfying (23) with κ replaced by ρ (since $\rho \geq \kappa$), we have that $\mu_1^{-1} \leq C_m d$ for a mask-dependent constant C_m. □

Proof of Theorem 1.8 We first note that $\delta + (s+1)/2 < 5d/16 \leq K \leq 10d/21 < 2\delta$. Next, we apply Corollary 4.3 with s, r, δ, and all other parameters set as above. Next, we observe that $\mathbf{W}$ will be full rank given that it is a Vandermonde matrix. Therefore, $\sigma_{\min}(\mathbf{W}) > 0$ will always hold. Finally, we note that, for any choice of d and $b \leq \pi - a$, Proposition 3.4 guarantees the existence of a smooth and compactly supported mask $\tilde{m}$ with $\mu_2 > 0$. □

5 Empirical Evaluation

We now present numerical results demonstrating the efficiency and robustness of Algorithms 1 and 2. All code is publicly available for the sake of reproducibility.[4]

5.1 Empirical Evaluation of Algorithm 1

We begin by investigating the empirical performance of Algorithm 1 in recovering the following class of compactly supported C^∞-smooth test functions,

$$f(x) \coloneqq \sum_{j=1}^{J} \alpha_j\, \xi_{c_1,c_2}(x - \nu_j). \tag{51}$$

Here $J \in \mathbb{N}$, $\alpha_j \in \mathbb{C}$, $\nu_j \in [-\pi, \pi]$, and ξ_{c_1,c_2} denotes a C^∞-smooth bump function with $\xi_{c_1,c_2}(x) > 0$ in (c_1, c_2) and $\xi_{c_1,c_2}(x) = 0$ for $x \notin [c_1, c_2]$. We may generate such a bump function (see, for example [30, Chapter 2]) as follows:

$$\xi_{c_1,c_2}(x) = \xi\left(-2 + 4\frac{x - c_1}{c_2 - c_1}\right), \qquad \xi(x) = \frac{h(2 - |x|)}{h(2 - |x|) + h(|x| - 1)}, \tag{52}$$

[4] Numerical implementations of the methods proposed here are available at https://bitbucket.org/charms/blockpr.

where

$$h(x) = \begin{cases} \mathrm{e}^{-1/x^2}, & x > 0, \\ 0, & x \leq 0. \end{cases}$$

For the experiments below, we set $J = 4$, $c_1 = -\pi/5$, $c_2 = \pi/5$, and choose α_j such that its real and complex components are both i.i.d. uniform random variables $\mathcal{U}[-1, 1]$. The shifts ν_j are selected uniformly at random (without repetition) from the set $\{-\nu_{\max} + j(2\nu_{\max}/(2J-1))\}_{j=0}^{2J-1}$ where $\nu_{\max} = 0.9\pi - \max\{|c_1|, |c_2|\}$ so that $\mathrm{supp}(f) \subseteq [-\pi, \pi]$. A representative plot of (the real and imaginary parts of) such a test function is provided in Fig. 1a.

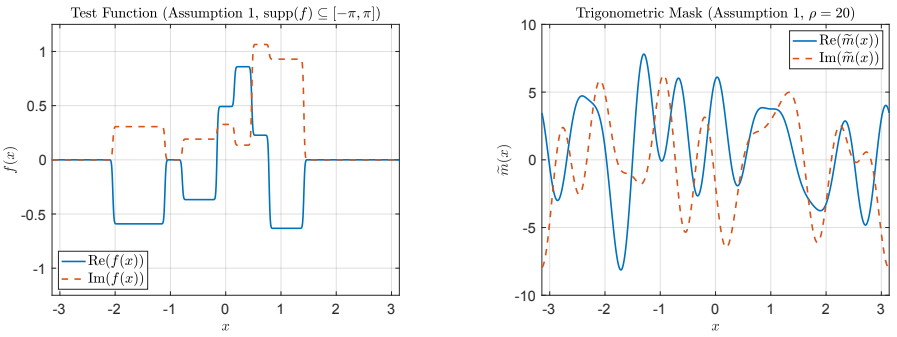

(a) Test Function (with $\mathrm{supp}(f) \subseteq [-\pi, \pi]$)

(b) Mask (Trigonometric Polynomial; $\rho = 20$)

Fig. 1: Representative Test Function and Mask Satisfying Assumption 1.

To generate masks satisfying Assumption 1 (see Section 1.1), we choose the Fourier coefficients $\widehat{m}$ from a zero mean, unit variance i.i.d. complex Gaussian distribution and empirically verify that the mask-dependent constant μ_1 (as defined in (22) is strictly positive. Fig. 1b plots such a (complex) trigonometric mask for $\rho = 20$, where $\rho + 1$ is the (two-sided) bandwidth of the mask. Table 1 lists the empirically calculated μ_1 values, and averaged over 100 trials) for such masks. The left two columns of the table list μ_1 for a fixed discretization size ($d = 211$) and varying ρ; they show that μ_1 is approximately constant for fixed d. The right two columns list μ_1 values for fixed ρ and varying d; they show μ_1 decreases slowly with d (roughly proportional to $1/d$). This verifies that constructing admissible (i.e., with $\mu_1 \neq 0$) trigonometric masks as per Assumption 1 is indeed possible for reasonable values of d and ρ.

Finding closed form analytical expressions for the integral in (7) is non-trivial. Therefore, we use numerical quadrature computations on an equispaced fine grid (of $10,001$ points) in $[-\pi, \pi]$ to generate phaseless measurements corresponding to (7) under both Assumptions 1 and 2.

We now investigate the noise robustness of Algorithm 1. For the results shown in Fig. 2a (where each data point is generated by averaging the results

$(d = 211, \rho)$	μ_1 (Average over 100 trials)	$(d, \rho = 50)$	μ_1 (Average over 100 trials)
$(211, 20)$	1.957×10^{-4}	$(111, 50)$	4.825×10^{-4}
$(211, 40)$	1.704×10^{-4}	$(223, 50)$	1.560×10^{-4}
$(211, 60)$	1.563×10^{-4}	$(447, 50)$	6.199×10^{-5}
$(211, 80)$	1.500×10^{-4}	$(895, 50)$	2.162×10^{-5}
$(211, 100)$	1.530×10^{-4}	$(1791, 50)$	8.247×10^{-6}

Table 1: Empirically evaluated μ_1 values (mask constant) for Algorithm 1. (Fourier coefficients of mask chosen as i.i.d. complex standard normal entries. Left two columns show μ_1 values for fixed d, right two columns show μ_1 values for fixed ρ.)

of 100 trials), we add i.i.d. random (real) Gaussian noise to the phaseless measurements (7) at desired signal to noise ratios (SNRs). In particular, the noise matrix $\boldsymbol{\eta}_{\mathbf{K},\mathbf{L}} \in \mathbb{R}^{d \times L}$ in Section 3 is chosen to be i.i.d. $\mathcal{N}(\mathbf{0}, \sigma^2 \mathbf{I})$. The variance σ^2 is chosen such that

$$\text{SNR (dB)} = 10 \log_{10} \left(\frac{\|\mathbf{Z}\|_F^2}{dL\,\sigma^2} \right)$$

where $\mathbf{Z}$ denotes the corresponding matrix of perfect (noiseless) measurements. Errors in the recovered signal are also reported in dB with

$$\text{Error (dB)} = 10 \log_{10} \left(\frac{h \sum_{i=0}^{N} |f(x_i) - f_e(x_i)|^2}{h \sum_{i=0}^{N} |f(x_i)|^2} \right),$$

where f and f_e denote the true and recovered functions respectively, and x_i denotes (equispaced) grid points in $[-\pi, \pi]$, i.e. $x_i = -\pi + hi$ with $h := 2\pi/N$. Errors reported in this section use $N = 2003$. MATLAB code used to generate these numerical results is freely available at [26].

Fig. 2a plots the error in recovering a test function using Algorithm 1 (for $d = 257, \rho = 32, \kappa = \rho - 1$ and $(2\rho - 1)d$ total measurements) over a wide range of SNRs. For reference, we also include results using an improved reconstruction method based on Algorithm 1, as well as the popular HIO+ER alternating projection algorithm [9, 27, 28]. Refinements over Algorithm 1 included use of an improved eigenvector-based magnitude estimation procedure in place of Step 6 (see [29, Section 6.1] for details), and (exponential) low-pass filtering[5] in the output Fourier partial sum reconstruction step of Algorithm 1. Fig. 2b plots the execution time (in seconds, averaged over 100 trials) to recover a test signal using dL measurements, where d is the discretization size, $L = 2\rho - 1$ and $\rho = \min\{(d-5)/2, 2\lfloor \log_2(d) \rfloor\}$. Both Algorithm 1 and its refined variant are essentially $\mathcal{O}(dL)$, where dL is the number of measurements acquired, with Algorithm 1 performing much faster than the HIO+ER procedure. Finally, we note that reconstruction error can be reduced by increasing the number

[5] With filter order increasing with SNR; we used a 2^{nd}-order filter at 10dB SNR and a 12^{th}-order filter at 60dB SNR.

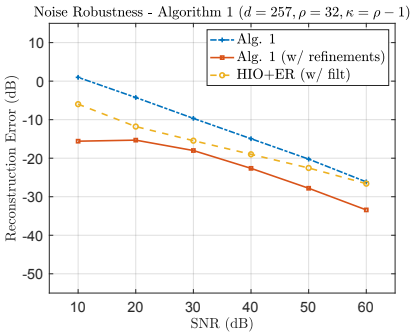

(a) Noise Robustness

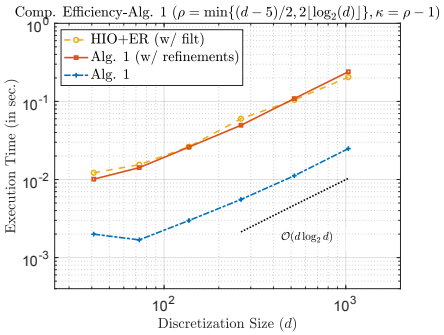

(b) Computational Cost

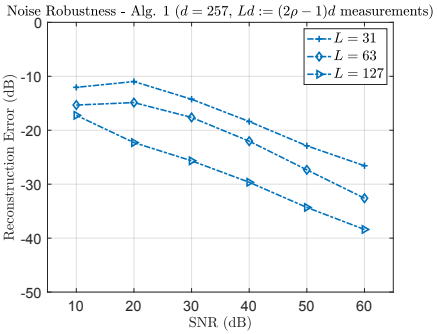

(c) Error vs. No. of Shifts

Fig. 2: Empirical Evaluation of Algorithm 1. Note in Fig. 2a that the refined version of Alg. 1 achieves lower reconstruction errors than HIO+ER. In Fig. 2b one can also see that Alg. 1 with no refinements is much faster than HIO+ER thereby demonstrating its value as a provably accurate way to quickly initialize such iterative methods.

of shifts L acquired (and consequently, the total number of measurements). Fig. 2c plots the error in reconstructing a test signal discretized using $d = 257$ points, $\kappa = \rho - 1$ and $Ld = (2\rho - 1)d$ measurements for different values of ρ (and correspondingly L). As expected, we see that noise performance improves as L increases.

For results utilizing the HIO+ER algorithm, we chose the zero vector as an initial guess, although use of a random starting guess did not change the qualitative nature of the results. As is common practice, (see for example [9]) we implemented the HIO+ER algorithm in "blocks" of eight HIO iterations followed by two ER iterations in order to accelerate convergence of the algorithm. Fig. 3a – which plots the HIO+ER reconstruction error (for the problem setting corresponding to Algorithm 1) against the total number of HIO+ER

iterations – illustrates the choice of these parameters. To minimize computational cost while ensuring convergence, the total number of HIO+ER iterations was limited to 30.

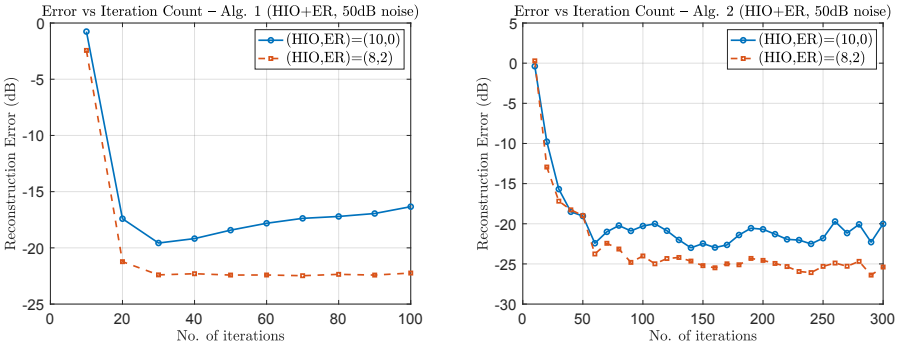

(a) Selection of HIO+ER Iteration parameters for Algorithm 1

(b) Selection of HIO+ER Iteration parameters for Algorithm 2

Fig. 3: Selection of HIO+ER Parameters for Algorithms 1 and 2. The notation (HIO,ER)=(x,y) denotes implementation of the HIO+ER algorithm in "blocks" of x iterations of the HIO algorithm followed by y iterations of the ER algorithm. A total of 30 and 100 iterations were used respectively for the simulations in Fig. 2 and Fig. 5 (in blocks of 8 HIO iterations followed by 2 ER iterations).

In summary, Algorithm 1 is significantly faster than the popular HIO+ER algorithm, although the reconstruction error is a bit larger. This demonstrates a trade off between speed and noise robustness. In practice, one might use a hybrid method in which one first applies Algorithm 1 as a computationally efficient initializer before then applying an iterative method such as HIO+ER. Alternatively, one could also use the modified version of Algorithm 1. Our experiments show that this modified algorithm is more accurate than HIO+ER while having nearly identical computational cost. Additional numerical experiments studying the convergence behavior of Algorithm 1 (in the absence of measurement errors) can be found in Appendix D.

5.2 Empirical Evaluation of Algorithm 2

We next present empirical simulations evaluating the robustness and efficiency of Algorithm 2. As detailed in Assumption 2 (see Section 1.1), we recover compactly supported test functions with $\mathrm{supp}(f) \subseteq (-a, a)$ using compactly supported masks which satisfy $\mathrm{supp}(\widetilde{m}) \subseteq (-b, b)$, where $a + b < \pi$. For experiments in this section, we choose $b = 3/4$ and $a = 0.9(\pi - 3/4)$. The test functions are generated as detailed in (51) of Section 5.1, as a (complex)

weighted sum of shifted C^∞-smooth bump functions, but with a maximum shift of $\nu_{\max} = a - b$. A representative test function is plotted in Fig. 4a. The corresponding compactly supported masks are generated as the product of a trigonometric polynomial and a bump function using

$$\widetilde{m}(x) = \xi_{-b,b}(x) \cdot \left(\sum_{p=-\rho/2}^{\rho/2} \widehat{m}(p) \mathrm{e}^{\mathrm{i}px/b} \right), \tag{53}$$

where $\xi_{-b,b}$ is the C^∞-smooth bump function described in Section 5.1, and the term in the parenthesis describes a (complex) $2b$-periodic trigonometric polynomial. A representative example of such as mask is provided in Fig. 4b with $\rho = 16$ and the coefficients $\widehat{m}$ chosen from a zero mean, unit variance i.i.d. complex Gaussian distribution.

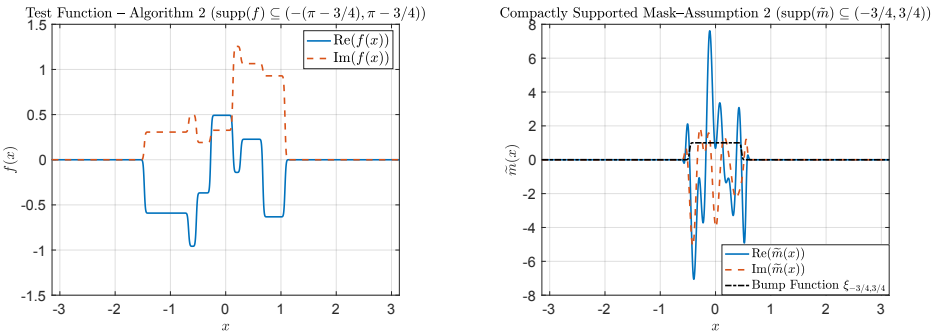

(a) Test Function ($a = \pi - 3/4$; $\mathrm{supp}(f) \subseteq (-a, a)$)

(b) Mask ($\mathrm{supp}(\widetilde{m}) \subseteq (-b, b) = (-3/4, 3/4)$)

Fig. 4: Representative Test Function and Mask Satisfying Assumption 2.

$(d = 189, \kappa)$	μ_2 (Average over 100 trials)	$(d, \kappa = 27)$	μ_2 (Average over 100 trials)
$(189, 3)$	2.563×10^{-3}	$(165, 27)$	9.722×10^{-5}
$(189, 10)$	2.873×10^{-4}	$(223, 27)$	8.866×10^{-5}
$(189, 31)$	8.331×10^{-5}	$(495, 27)$	4.686×10^{-5}
$(189, 94)$	2.642×10^{-19}	$(1045, 27)$	2.448×10^{-5}

Table 2: Empirically evaluated μ_2 values (mask constant) for Algorithm 2. The left two columns show μ_2 values for fixed d, right two columns show μ_2 values for fixed κ. Here, $\delta = \kappa + 1$ and $s = \kappa - 1$.

Representative values of the mask constant μ_2 (as defined in (36) and averaged over 100 trials) are listed in Table 2. The first two columns list μ_2 values for fixed discretization size d, while the last two columns list μ_2 values for fixed

κ. In both cases, we set $K = 2\kappa+1$ and ensure that K divides d. We note that κ denotes the number of modes used in the Wigner deconvolution procedure (Step 2) in Algorithm 2. Since the masks constructed using (53) are compactly supported and smooth, we expect the autocorrelation of their Fourier transforms (and the corresponding Fourier coefficients of this autocorrelation) to decay rapidly. Therefore, we expect μ_2 to be small for large κ values; indeed, this is seen in the last row of Table 2 where the μ_2 value is essentially zero when $d = 189, \kappa = 94$. However, as the functions we expect to recover also exhibit rapid decay in Fourier coefficients, we only require a small number of their Fourier modes to ensure accurate reconstructions. Hence, small to moderate κ values suffice. As seen in Table 2, it is feasible to construct admissible masks (i.e., $\mu_2 > 0$) for such (d, κ) pairs. Experiments have also been conducted with $\widetilde{m}$ chosen to be the bump function $\xi_{-b,b}$ and a (truncated) Gaussian, However, these experiments yield smaller mask constants μ_2, which make the resulting reconstructions more susceptible to noise. Selection of "optimal" and physically realizable compactly supported masks is an open problem which we defer to future research.

We note that due to the equivalence of (34) and (35), the Wigner deconvolution step (Step 2) in Algorithm 2 may be instead evaluated using (34). While theoretical analysis of this equivalent procedure is more involved, it offers computational advantages since it does not require solving[6] the Vandermonde system of Step 4 in Algorithm 2. The corresponding μ_2 values for this procedure also follow the qualitative behavior in Table 2. This variant of Algorithm 2 is used in generating some of the plots in Appendix D, while Fig. 5 provides a comparison of Algorithm 2 and this alternate implementation.

We now study the robustness and computational efficiency of Algorithm 2. Fig. 5a plots the error in recovering a test function (with each data point averaged over 100 trials) for discretization size $d = 189$, $\delta = 32$, $\kappa = \delta - 1$, $s = 29$ and $d/3$ total measurements over a wide range of SNRs. For reference, we also include results using the HIO+ER alternating projection algorithm, as well as the alternate implementation of Algorithm 2 (using (34) to implement the Wigner deconvolution Step 2). As in Section 5.1, the alternate implementation of Algorithm 2 and the HIO+ER implementations utilize (exponential) low-pass filtering. The HIO+ER algorithm is implemented in blocks of eight HIO iterations followed by two ER iterations in order to accelerate the convergence of the algorithm, with a total of 100 iterations used to ensure convergence while minimizing computational cost (see Fig. 3b). Additionally, we also provide results using a post-processed implementation of Algorithm 2 using just 10 iterations of HIO+ER. Since this method only uses 10 HIO+ER iterations (rather than 100), it has a lower overall computational cost than the pure HIO+ER method. Therefore, in this context, we can view the proposed method as an initializer which accelerates the convergence of alternating projection algorithms such as HIO+ER. Finally, Fig. 5b, which plots the execution time

[6] We use the *Iterated Tikhonov* method (see [31], [8, Algorithm 3]) to invert the Vandermonde system in Step 4 of Alg. 2.

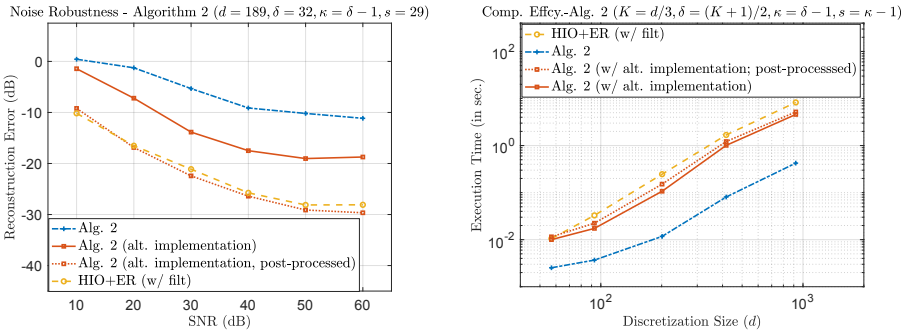

(a) Noise Robustness (b) Computational Cost

Fig. 5: Empirical Evaluation of Algorithm 2. In Fig. 4a Algorithm 2 with alternate implementation and post-processing (red dotted curve) demonstrates that using Alg. 2 to initialize HIO+ER allows just 10 subsequent iterations of HIO+ER to converge to a more accurate approximation than 100 iterations of HIO+ER with standard initialization (yellow dashed curve). In addition to achieving a lower reconstruction error, Fig. 4b shows that the Algorithm 2 initialized version of HIO+ER is also faster than the standard initialized version. The end result is that initializing HIO+ER with Algorithm 2 allows better reconstructions more quickly than standard initialization does.

(in seconds, averaged over 100 trials) to recover a test signal, shows that the proposed method in Algorithm 2 and its alternate implementation are computationally efficient, with all implementations running in $\mathcal{O}(dK)$ time where dK is the number of measurements acquired. Overall, similar to Algorithm 1, we see that Algorithm 2 is significantly faster than HIO+ER. Moreover, the modified version which includes post-processing has slightly better accuracy than HIO+ER while also having a slightly lower computational cost.

Acknowledgments. Mark Iwen was supported in part by NSF DMS 1912706. Nada Sissouno acknowledges partial funding from an Entrepreneurial Award in the Program "Global Challenges for Women in Math Science" funded by the Faculty of Mathematics at the Technical University of Munich. Aditya Viswanathan was supported in part by NSF DMS 2012238.

Appendix A The Proofs of Lemma 2.3

Proof Let $g \coloneqq P_{\mathcal{S}} f$ and $h \coloneqq P_{\mathcal{R}} m$, where $P_{\mathcal{S}}$ and $P_{\mathcal{R}}$ are the Fourier projection operators defined as in (11). Since g and h are trigonometric polynomials and $\mathcal{R}+\mathcal{S} \subseteq \mathcal{D}$, we may write

$$\int_{-\pi}^{\pi} g(x)h(x-\tilde{\ell})\mathrm{e}^{-\mathrm{i}x\omega}dx$$

$$
\begin{aligned}
&= \sum_{m\in\mathcal{R}}\sum_{n\in\mathcal{S}} \widehat{g}(n)\widehat{h}(m)\mathbb{e}^{-\mathbb{i}m\tilde{\ell}} \int_{-\pi}^{\pi} \mathbb{e}^{\mathbb{i}(m+n-\omega)x}dx \\
&= \sum_{m\in\mathcal{R}}\sum_{n\in\mathcal{S}} \widehat{g}(n)\widehat{h}(m)\mathbb{e}^{-\mathbb{i}m\tilde{\ell}} \frac{2\pi}{d} \sum_{p\in\mathcal{D}} \mathbb{e}^{2\pi\mathbb{i}p(n+m-\omega)/d} \\
&= \frac{2\pi}{d} \sum_{p\in\mathcal{D}} \left(\sum_{n\in\mathcal{S}} \widehat{g}(n)\mathbb{e}^{2\pi\mathbb{i}pn/d} \right) \left(\sum_{m\in\mathcal{R}} \widehat{h}(m)\mathbb{e}^{\left(\left(\frac{2\pi\mathbb{i}m}{d}\right)(p-\ell)\right)} \right) \mathbb{e}^{-2\pi\mathbb{i}mp\omega/d} \\
&= \frac{2\pi}{d} \sum_{p\in\mathcal{D}} g\left(\frac{2\pi p}{d}\right) h\left(\frac{2\pi(p-\ell)}{d}\right) \mathbb{e}^{-2\pi\mathbb{i}p\omega/d} \\
&= \frac{2\pi}{d} \sum_{p\in\mathcal{D}} x_p y_{p-\ell} \mathbb{e}^{-2\pi\mathbb{i}\omega p/d}.
\end{aligned}
$$

□

Appendix B The Proofs of Propositions 3.2 and 3.4

The Proof of Proposition 3.2 We first note that

$$
\widehat{z}_q = \begin{cases} \widehat{m}(q) & \text{if } |q| \le \rho/2, \\ 0 & \text{if } |q| > \rho/2. \end{cases}
$$

Therefore, for all $|p| \le \kappa - 1$, we have

$$
\left(\widehat{\mathbf{z}} \circ S_p\overline{\widehat{\mathbf{z}}}\right)_q = \begin{cases} \widehat{m}(q)\widehat{m}(p+q) & \text{if } -\rho/2 \le q,\, p+q \le \rho/2, \\ 0 & \text{otherwise.} \end{cases}
$$

For any $|p| \le \kappa - 1$, let

$$
\mathcal{I}_p := \{q \in \mathcal{D} : -\rho/2 \le q \le \rho/2 \quad \text{and} \quad -\rho/2 \le q+p \le \rho/2\}.
$$

One may check that

$$
\mathcal{I}_p = \begin{cases} \left[-\frac{\rho}{2} - p, \frac{\rho}{2}\right] \cap \mathbb{Z} & \text{if } p < 0 \\ \left[-\frac{\rho}{2}, \frac{\rho}{2} - p\right] \cap \mathbb{Z} & \text{if } p \ge 0 \end{cases}.
$$

Therefore, making a simple change of variables in the case $p < 0$, we have that

$$
\mathbf{F_d}\left(\widehat{\mathbf{z}} \circ S_p\overline{\widehat{\mathbf{z}}}\right)_q = \frac{1}{d}\sum_{\ell\in\mathcal{I}_p} \widehat{m}(\ell)\widehat{m}(p+\ell)\mathbb{e}^{-2\pi\mathbb{i}q\ell/d} = \frac{1}{d}\sum_{\ell=-\rho/2}^{\rho/2-|p|} \widehat{m}(\ell)\widehat{m}\left(\ell+|p|\right)\mathbb{e}^{\mathbb{i}\phi_{p,q,\ell}},
$$

where $\mathbb{e}^{\mathbb{i}\phi_{p,q,\ell}}$ is a unimodular complex number depending on p, q and ℓ. Using the assumptions (23) and (24), we see that

$$
\begin{aligned}
\left|\frac{1}{d}\sum_{\ell=-\rho/2+1}^{\rho/2-|p|} \widehat{m}(\ell)\widehat{m}(\ell+|p|)\mathbb{e}^{\mathbb{i}\phi_{p,q,\ell}}\right| &\le \frac{\rho}{d}\left|\widehat{m}\left(\frac{-\rho}{2}+1\right)\right|\left|\widehat{m}\left(\frac{-\rho}{2}+1+|p|\right)\right| \\
&\le \frac{1}{2d}\left|\widehat{m}\left(\frac{-\rho}{2}\right)\right|\left|\widehat{m}\left(\frac{-\rho}{2}+|p|\right)\right|.
\end{aligned}
$$

With this, we may use the reverse triangle inequality to see

$$
\left|\mathbf{F_d}\left(\widehat{\mathbf{z}} \circ S_p\overline{\widehat{\mathbf{z}}}\right)_q\right| = \left|\frac{1}{d}\sum_{\ell=-\rho/2}^{\rho/2-|p|} \widehat{m}(\ell)\widehat{m}(\ell+|p|)\mathbb{e}^{\mathbb{i}\phi_{p,q,\ell}}\right|
$$

$$\geq \frac{1}{d}\left|\widehat{m}\left(\frac{-\rho}{2}\right)\right|\left|\widehat{m}\left(\frac{-\rho}{2}+|p|\right)\right| - \frac{1}{d}\left|\sum_{\ell=-\rho/2+1}^{\rho/2-|p|}\widehat{m}(\ell)\widehat{m}(\ell+|p|)\mathbb{e}^{\mathbb{i}\phi_{p,q,\ell}}\right|$$
$$\geq \frac{1}{2d}\left|\widehat{m}\left(\frac{-\rho}{2}\right)\right|\left|\widehat{m}\left(\frac{-\rho}{2}+|p|\right)\right|$$
$$\geq \frac{1}{2d}\left|\widehat{m}\left(\frac{-\rho}{2}\right)\right|\left|\widehat{m}\left(\frac{-\rho}{2}+\kappa-1|\right)\right|.$$

□

The Proof of Proposition 3.4 First, we note that by applying Lemma 3.3, and setting $p=\omega, q=\ell$, we have

$$\begin{aligned}\mu_2 &= \inf_{\omega\in[2\kappa-1]_c,\ell\in[2s-1]_c}|(\mathbf{F_d}(\widehat{\mathbf{z}}\circ S_\ell\overline{\widehat{\mathbf{z}}}))_\omega|\\ &= \frac{1}{d}\inf_{\omega\in[2\kappa-1]_c,\ell\in[2s-1]_c}|(\mathbf{F_d}(\mathbf{z}\circ S_\omega\overline{\mathbf{z}}))_\ell|\\ &= \frac{1}{d}\inf_{p\in[2\kappa-1]_c,q\in[2s-1]_c}|(\mathbf{F_d}(\mathbf{z}\circ S_p\overline{\mathbf{z}}))_q|.\end{aligned}$$

For $|p|\leq\kappa-1$, we have

$$(\mathbf{z}\circ S_p\overline{\mathbf{z}})_q = \begin{cases} z_q\overline{z_{p+q}} & \text{if } n\leq q, p+q\leq n+\tilde{\delta}-1,\\ 0 & \text{otherwise.}\end{cases}$$

For any $|p|\leq\kappa-1$, let

$$\mathcal{I}_p := \{q\in\mathcal{D}: n\leq q\leq n+\tilde{\delta}-1 \quad\text{and}\quad n\leq q+p\leq n+\tilde{\delta}-1\}.$$

One may check that

$$\mathcal{I}_p = \begin{cases}[n-p, n+\tilde{\delta}-1]\cap\mathbb{Z} & \text{if } p<0,\\ [n, n+\tilde{\delta}-1-p]\cap\mathbb{Z} & \text{if } p\geq 0.\end{cases}$$

Therefore, making a simple change of variables in the case $p<0$, we have that in either case

$$\left|\mathbf{F_d}\left(\mathbf{z}\circ S_p\overline{\mathbf{z}}\right)_q\right| = \frac{1}{d}\left|\sum_{\ell\in\mathcal{I}_p} z_\ell\overline{z_{p+\ell}}\mathbb{e}^{-2\pi\mathbb{i}\ell q/d}\right| = \frac{1}{d}\left|\sum_{\ell=n}^{n+\tilde{\delta}-1-|p|} z_\ell\overline{z_{\ell+|p|}}\mathbb{e}^{\mathbb{i}\phi_{p,q,\ell}}\right|,$$

where $\mathbb{e}^{\mathbb{i}\phi_{p,q,\ell}}$ is a unimodular complex number depending on p, q and ℓ. Using the assumptions (37) and (38) we see that

$$\left|\frac{1}{d}\sum_{\ell=n+1}^{n+\tilde{\delta}-1-|p|} z_\ell\overline{z_{\ell+|p|}}\mathbb{e}^{\mathbb{i}\phi_{p,q,\ell}}\right| \leq \frac{\tilde{\delta}}{d}|z_{n+1}|\left|z_{n+1+|p|}\right| \leq \frac{1}{2d}|z_n||z_{n+|p|}|.$$

With this,

$$\begin{aligned}\left|F_d\left(\mathbf{z}\circ S_p\overline{\mathbf{z}}\right)_q\right| &= \left|\frac{1}{d}\sum_{\ell=n}^{n+\tilde{\delta}-1-|p|} z_\ell\overline{z_{\ell+|p|}}\mathbb{e}^{\mathbb{i}\phi_{p,q,\ell}}\right|\\ &\geq \frac{1}{d}|z_n||z_{n+|p|}| - \left|\frac{1}{d}\sum_{\ell=n+1}^{n+\tilde{\delta}-1-|p|} z_\ell\overline{z_{\ell+|p|}}\mathbb{e}^{\mathbb{i}\phi_{p,q,\ell}}\right|\\ &\geq \frac{1}{2d}|z_n||z_{n+|p|}| \geq \frac{1}{2d}|z_n||z_{n+\kappa-1}|.\end{aligned}$$

Thus, the proof is complete. □

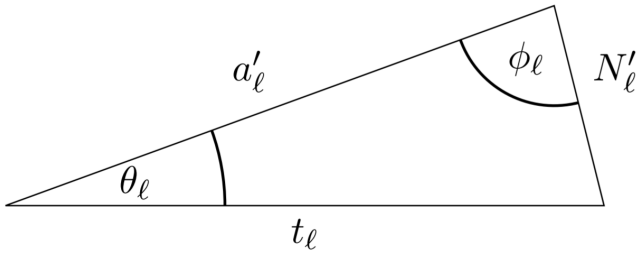

Fig. C1: Triangle in the complex domain.

Appendix C The Proof of Lemma 4.5

Proof Our proof requires the following sublemma which shows that, if $n \in L_f$, then Algorithm 3 used in the definition of α_n will only select indices n_ℓ corresponding to large Fourier coefficients.

Lemma C.1 *Let $n \in L_f$, and let $n_0, \dots, n_\zeta$ be the sequence of indices as introduced in the definition of α_n. Then*

$$|\widehat{f}(n_\ell)| \geq \frac{|\widehat{f}(n)|}{2}$$

for all $0 \leq \ell \leq \zeta$.

Proof When $\ell = \zeta$, the claim is immediate from the fact that $n_\zeta = n$. For all $0 \leq \ell \leq \zeta - 1$, the definition of n_ℓ implies that there exists an interval I_ℓ, centered at some point a with $|a| \leq |n|$, such that the length of I_ℓ is at most β and

$$a_{n_\ell} = \max_{m \in I_\ell} a_m.$$

Letting $\epsilon = \sqrt{3\|\mathbf{N}\|_\infty}$, we see that by (45) and Remark 1.5

$$|\widehat{f}(n_\ell)| \geq a_{n_\ell} - \epsilon = \max_{m \in I_\ell} a_m - \epsilon \geq \max_{m \in I_\ell} |\widehat{f}(m)| - 2\epsilon \geq |\widehat{f}(n)| - 2\epsilon.$$

The result now follows from noting that $\epsilon < \frac{|\widehat{f}(n)|}{4}$ for all $n \in L_f$. □

With Lemma C.1 established, we may now prove Lemma 4.5. Let $n \in L_f$ and let $n_0, \dots n_\zeta$ be the sequence describe in the definition of α_n. For $0 \leq \ell \leq \zeta - 1$, let $t_\ell \coloneqq \widehat{f}(n_{\ell+1})\overline{\widehat{f}(n_\ell)}$, $a'_\ell \coloneqq \widehat{f}(n_{\ell+1})\overline{\widehat{f}(n_\ell)} + N_{n_{\ell+1}, n_\ell}$, and $N'_\ell \coloneqq N_{n_{\ell+1}, n_\ell}$. Consider the triangle with sides a'_ℓ, t_ℓ, and N'_ℓ with angles $\theta_\ell = |\arg(a'_\ell) - \arg(t_\ell)|$ and $\phi_\ell = |\arg(a'_\ell) - \arg(N'_\ell)|$, as illustrated in Figure C1.

By the law of sines and Lemma C.1, we get that

$$|\sin(\theta_\ell)| = \left| \frac{N'_\ell}{t_\ell} \sin(\phi_\ell) \right| \leq \frac{\|\mathbf{N}\|_\infty}{|\widehat{f}(n_\ell)||\widehat{f}(n_{\ell+1})|} \leq \frac{4\|\mathbf{N}\|_\infty}{|\widehat{f}(n)|^2} \tag{C1}$$

for all $0 \leq \ell \leq \zeta$. By the definition of L_f and Lemma C.1, we have that for all ℓ

$$|N'_\ell| \leq \|\mathbf{N}\|_\infty \leq \frac{|\widehat{f(n)}|^2}{4} \leq |\widehat{f}(n_\ell)||\widehat{f}(n_{\ell+1})| = |t_\ell|.$$

Therefore, $0 \leq \theta_\ell \leq \frac{\pi}{2}$, and so by (C1), we have

$$|\theta_\ell| \leq \frac{\pi}{2} |\sin(\theta_\ell)| \leq 2\pi \frac{\|\mathbf{N}\|_\infty}{|\widehat{f}(n)|^2}.$$

By definition $\tau_n = \sum_{\ell=0}^{\zeta-1} \arg(t_\ell)$ and $\alpha_n = \sum_{l=0}^{\zeta-1} \arg(a'_\ell)$. Therefore, we have

$$|\mathrm{e}^{\mathrm{i}\tau_n} - \mathrm{e}^{\mathrm{i}\alpha_n}| \leq |\alpha_n - \tau_n| = \left| \sum_{\ell=0}^{\zeta-1} \arg(a'_\ell) - \arg(t_\ell) \right| = \left| \sum_{\ell=0}^{\zeta-1} \theta_\ell \right| \leq 2\pi b \frac{\|\mathbf{N}\|_\infty}{|\widehat{f}(n)|^2}.$$

From the definition of n_ℓ, we have

$$|n_\ell - n_{\ell-1}| \geq \gamma - \beta \geq \frac{\gamma}{2}$$

for all $1 \leq \ell \leq \zeta - 1$. Therefore, the path length ζ is bounded by

$$\zeta \leq \frac{|n - n_0|}{\min |n_\ell - n_{\ell-1}|} \leq \frac{2d}{\gamma}.$$

Thus, we have

$$|\mathrm{e}^{\mathrm{i}\tau_n} - \mathrm{e}^{\mathrm{i}\alpha_n}| \leq 2\pi b \frac{\|\mathbf{N}\|_\infty}{|\widehat{f}(n)|^2} \leq \frac{4\pi d}{\gamma} \frac{\|\mathbf{N}\|_\infty}{|\widehat{f}(n)|^2}$$

as desired.

□

Appendix D Additional Experiments

In this section, we provide additional numerical simulations studying the empirical convergence behavior of Algorithms 1 and 2. We start with a study of the convergence behavior of Algorithm 1. Here, we reconstruct the same test function using different discretization sizes d (with ρ chosen to be $\min\{(d-5)/2, 16\lfloor \log_2(d) \rfloor\}$ and $\kappa = \rho - 1$), where the total number of phaseless measurements used is $Ld = (2\rho - 1)d$. Fig. D2 plots representative reconstructions (of the real part of the test function) for two choices of d ($d = 33$ and $d = 1025$). We note that the (smooth) test function illustrated in the figure has several sharp and closely separated gradients, making the reconstruction process challenging. This is evident in the partial Fourier sums ($P_N f$) plotted for reference alongside the reconstructions from Algorithm 1 (f_e). For small d and ρ, we observe oscillatory behavior similar to that seen in the Gibbs phenomenon. Nevertheless, we see that the proposed algorithm closely tracks the performance of the partial Fourier sum, with reconstruction quality improving significantly as d (and ρ) increases.

We next evaluate the convergence behavior of Algorithm[7] 2 by reconstructing the same test function using different discretization sizes d (with $K = d/3$, $\delta = (K+1)/2$, $\kappa = \delta - 1$ and $s = \kappa - 1$). Fig. D3 plots representative reconstructions (of the real part of the test function) for two choices of d ($d = 57$ and $d = 921$). As in Fig. D2, we note that the (smooth) test function has

[7] using the alternate implementation – with (34) utilized in place of (35) in Step 2 of the Algorithm – as described in Section 5

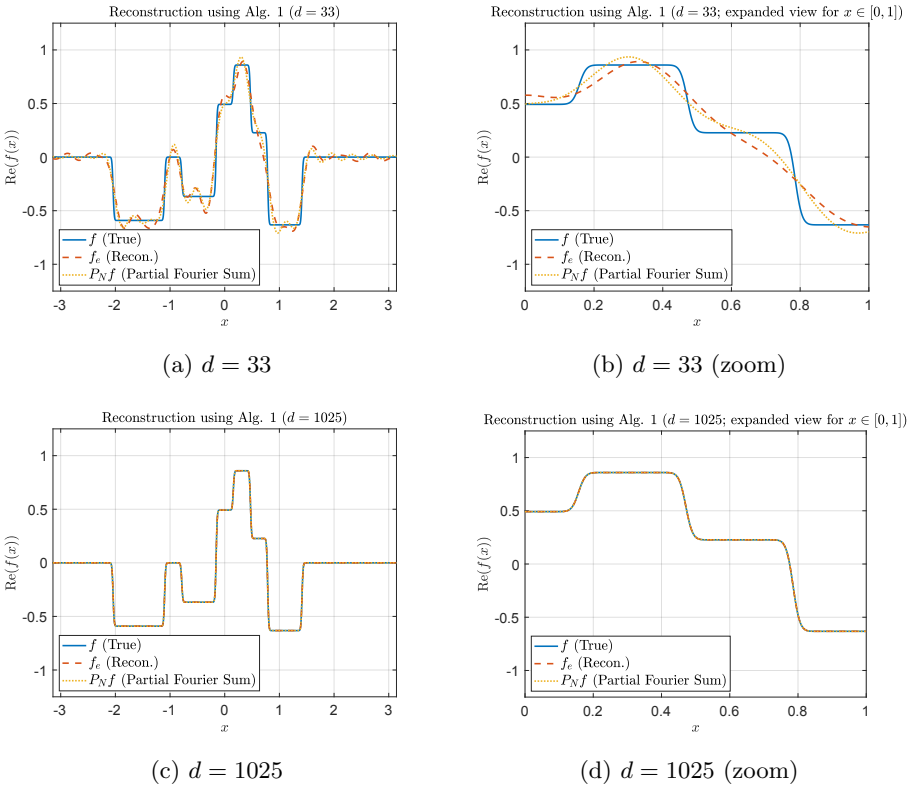

(a) $d = 33$ (b) $d = 33$ (zoom)

(c) $d = 1025$ (d) $d = 1025$ (zoom)

Fig. D2: Evaluating the convergence behavior of Algorithm 1. Figure plots reconstructions of the real part of the test function at $d = 33$ and $d = 1025$ (along with an expanded view of the reconstruction in $[0, 1]$) on a discrete equispaced grid in $[-\pi, \pi]$ of 7003 points; we set $\rho = \min\{(d-5)/2, 16\lfloor \log_2(d) \rfloor\}$ and $\kappa = \rho - 1$.

several sharp and closely separated gradients, making the reconstruction process challenging. Again, the partial Fourier sums ($P_N f$) plotted alongside the reconstructions from Algorithm 2 (f_e) exhibit Gibbs-like oscillatory behavior for small d and κ. Nevertheless, we see that the proposed algorithm closely tracks the performance of the partial Fourier sum, with reconstruction quality improving significantly as d (and δ, κ) increases.

Appendix E Results from Previous Work

The following is a restatement of Theorem 4 of [8] updated to use the notation of this paper. Notably, in this paper we use a different normalization of the Fourier transform (our $\mathbf{F_d}$ is equal to the F_d from [8] divided by d). We also note that the measurements $\mathbf{T}'$ considered here differ by a factor of $\frac{4\pi}{d^2}$ from

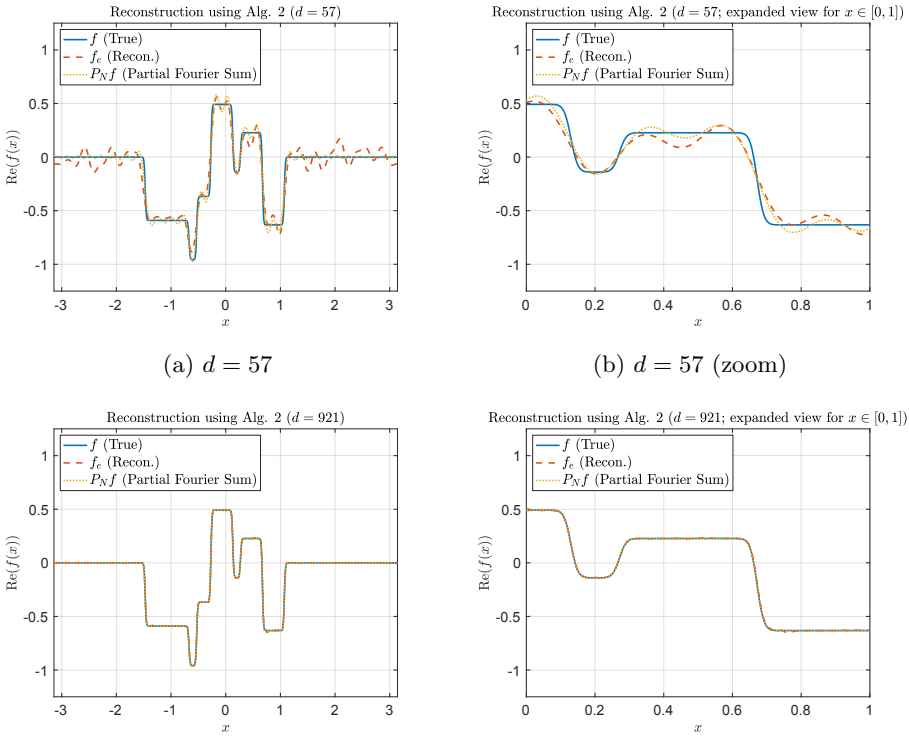

(a) $d = 57$ (b) $d = 57$ (zoom)

(c) $d = 921$ (d) $d = 921$ (zoom)

Fig. D3: Evaluating the convergence behavior of Algorithm 2. Figure plots reconstructions of the real part of the test function at $d = 57$ and $d = 921$ (along with an expanded view of the reconstruction in $[0, 1]$) on a discrete equispaced grid in $[-\pi, \pi]$ of 7003 points; we set $K = d/3, \delta = (K + 1)/2$ and $\kappa = \delta - 1$.

the measurements Y considered in [8]. Lastly, we note that the summations in [8] take place over a different string of d consecutive integers. However, this makes no difference do the the periodicity of the complex exponential function.

Theorem E.1 (Theorem 4 of [8]) *Let* $\tilde{\mathbf{T}}$ *be as in* (16). *Then for any* $\omega \in [K]_c$ *and* $\ell \in [L]_c$,

$$\begin{aligned}
&\frac{\widetilde{T}_{\ell,\omega} - \widetilde{N}_{\ell,\omega}}{4\pi^2} \\
=&d \sum_{p \in \left[\frac{d}{K}\right]_c} \sum_{q \in \left[\frac{d}{L}\right]_c} \left(\mathbf{F_d}\left(\widehat{\mathbf{x}} \circ S_{qL-\ell}\overline{\widehat{\mathbf{x}}}\right)\right)_{\omega - pK} \left(\mathbf{F_d}\left(\widehat{\mathbf{m}} \circ S_{\ell - qL}\overline{\widehat{\mathbf{m}}}\right)\right)_{\omega - pK} \\
=&\frac{1}{d} \sum_{p \in \left[\frac{d}{K}\right]_c} \sum_{q \in \left[\frac{d}{L}\right]_c} \mathrm{e}^{-2\pi \mathrm{i}(qL-\ell)(\omega - pK)/d} \left(\mathbf{F_d}\left(\widehat{\mathbf{x}} \circ S_{qL-\ell}\overline{\widehat{\mathbf{x}}}\right)\right)_{\omega - pK} \left(\mathbf{F_d}\left(\mathbf{m} \circ S_{\omega - pK}\overline{\mathbf{m}}\right)\right)_{qL-\ell}
\end{aligned}$$

$$= \frac{1}{d} \sum_{p \in \left[\frac{d}{K}\right]_c} \sum_{q \in \left[\frac{d}{L}\right]_c} \mathbb{e}^{2\pi \mathbb{i}(qL-\ell)(\omega - pK)/d} \left(\mathbf{F_d}\left(\mathbf{x} \circ S_{\omega - pK}\overline{\mathbf{x}}\right)\right)_{\ell - qL} \left(\mathbf{F_d}\left(\widehat{\mathbf{m}} \circ S_{\ell - qL}\overline{\widehat{\mathbf{m}}}\right)\right)_{\omega - pK}$$

$$= \frac{1}{d} \sum_{p \in \left[\frac{d}{K}\right]_c} \sum_{q \in \left[\frac{d}{L}\right]_c} \left(\mathbf{F_d}\left(\mathbf{x} \circ S_{\omega - pK}\overline{\mathbf{x}}\right)\right)_{\ell - qL} \left(\mathbf{F_d}\left(\mathbf{m} \circ S_{\omega - pK}\overline{\mathbf{m}}\right)\right)_{qL - \ell}.$$

References

[1] Walther, A.: The question of phase retrieval in optics. Optica Acta: Int. J. Opt. **10**(1), 41–49 (1963) https://doi.org/10.1080/713817747

[2] Fienup, C., Dainty, J.: Phase retrieval and image reconstruction for astronomy. Image Recovery: Theory and Application, 231–275 (1987)

[3] Griffin, D., Lim, J.: Signal estimation from modified short-time fourier transform. IEEE Transactions on Acoustics, Speech, and Signal Processing **32**(2), 236–243 (1984)

[4] Balan, R., Casazza, P., Edidin, D.: On signal reconstruction without phase. Applied and Computational Harmonic Analysis **20**(3), 345–356 (2006)

[5] Rodenburg, J.: Ptychography and related diffractive imaging methods. Advances in Imaging and Electron Physics **150**, 87–184 (2008)

[6] Candès, E.J., Eldar, Y.C., Strohmer, T., Voroninski, V.: Phase retrieval via matrix completion. SIAM review **57**(2), 225–251 (2015)

[7] Candès, E.J., Li, X., Soltanolkotabi, M.: Phase retrieval from coded diffraction patterns. Applied and Computational Harmonic Analysis **39**(2), 277–299 (2015). https://doi.org/10.1016/j.acha.2014.09.004

[8] Perlmutter, M., Merhi, S., Viswanathan, A., Iwen, M.: Inverting spectrogram measurements via aliased wigner distribution deconvolution and angular synchronization. Information and Inference: A Journal of the IMA (2020). https://doi.org/10.1093/imaiai/iaaa023

[9] Fienup, J.R.: Phase retrieval algorithms: a comparison. Applied optics **21**(15), 2758–2769 (1982)

[10] Gerchberg, R.W., Saxton, W.O.: A Practical Algorithm for the Determination of Phase from Image and Diffraction Plane Pictures. Optik **35**, 237–246 (1972)

[11] Alexeev, B., Bandeira, A.S., Fickus, M., Mixon, D.G.: Phase Retrieval with Polarization. SIAM Journal on Imaging Sciences **7**(1), 35–66 (2014)

[12] Gross, D., Krahmer, F., Kueng, R.: Improved recovery guarantees for phase retrieval from coded diffraction patterns. Applied and Computational Harmonic Analysis **42**, 37–64 (2017)

[13] Forstner, A., Krahmer, F., Melnyk, O., Sissouno, N.: Well conditioned ptychograpic imaging via lost subspace completion. Inverse Problems (2020). arXiv preprint arXiv 2004.04458

[14] Rosenblatt, J.: Phase retrieval. Commun. Math. Phys. **95**, 317–343 (1984). https://doi.org/10.1007/BF01212402

[15] Akutowicz, E.J.: On the determination of the phase of a Fourier integral, I. Trans. Amer. Math. Soc. **83**(1), 179–192 (1956). https://doi.org/10.2307/1992910

[16] Akutowicz, E.J.: On the determination of the phase of a Fourier integral, II. Proc. Am. Math. Soc. **8**(2), 234–238 (1957). https://doi.org/10.2307/2033718

[17] Jaming, P.: Uniqueness results in an extension of Pauli's phase retrieval problem. Appl. Comput. Harmon. Anal. **37**(3), 413–441 (2014). https://doi.org/10.1016/j.acha.2014.01.003

[18] Alaifari, R., Wellershoff, M.: Uniqueness of stft phase retrieval for bandlimited functions. Applied and Computational Harmonic Analysis **50**, 34–48 (2021). https://doi.org/10.1016/j.acha.2020.08.003

[19] Cheng, C., Daubechies, I., Dym, N., Lu, J.: Stable phase retrieval from locally stable and conditionally connected measurements. arXiv preprint arXiv:2006.11709 (2020)

[20] Thakur, G.: Reconstruction of bandlimited functions from unsigned samples. J. Fourier Anal. Appl. **17**(4), 720–732 (2011)

[21] Gröchenig, K.: Phase-retrieval in shift-invariant spaces with gaussian generator. Journal of Fourier Analysis and Applications **26** (2020). https://doi.org/10.1007/s00041-020-09755-5

[22] Alaifari, R., Daubechies, I., Grohs, P., Yin, R.: Stable phase retrieval in infinite dimensions. Foundations of Computational Mathematics **19**(4), 869–900 (2019)

[23] Iwen, M.A., Merhi, S., Perlmutter, M.: Lower Lipschitz bounds for phase retrieval from locally supported measurements. Applied and Computational Harmonic Analysis (2019)

[24] Iwen, M.A., Viswanathan, A., Wang, Y.: Fast Phase Retrieval from

Local Correlation Measurements. SIAM Journal on Imaging Sciences **9**(4), 1655–1688 (2016). https://doi.org/10.1137/15m1053761

[25] Filbir, F., Krahmer, F., Melnyk, O.: On recovery guarantees for angular synchronization. arXiv preprint arXiv 2005.02032 (2020). https://arxiv.org/abs/2005.02032

[26] Viswanathan, A., Iwen, M., Wang, Y.: BlockPR: Matlab Software for Phase Retrieval using Block Circulant Measurement Constructions and Angular Synchronization, version 2.0. https://bitbucket.org/charms/blockpr (2016)

[27] Bauschke, H.H., Combettes, P.L., Luke, D.R.: Phase retrieval, error reduction algorithm, and Fienup variants: A view from convex optimization. Journal of the Optical Society of America. A, Optics, Image science, and Vision **19**(7), 1334–1345 (2002)

[28] Marchesini, S., Tu, Y.-C., Wu, H.-t.: Alternating projection, ptychographic imaging and phase synchronization. Applied and Computational Harmonic Analysis **41**(3), 815–851 (2016)

[29] Iwen, M.A., Preskitt, B., Saab, R., Viswanathan, A.: Phase retrieval from local measurements: improved robustness via eigenvector-based angular synchronization. Applied and Computational Harmonic Analysis **48**, 415–444 (2020)

[30] Lee, J.M.: Introduction to Smooth Manifolds, 2nd edn. Springer, New York, NY (2012). https://doi.org/10.1007/978-1-4419-9982-5

[31] Buccini, A., Donatelli, M., Reichel, L.: Iterated tikhonov regularization with a general penalty term. Numerical Linear Algebra with Applications **24**(4), 2089 (2017)